Chapter 3: Petrology

INTRODUCTION

Previous petrographic investigations of the Boggabri Volcanics have been brief. Jensen (1907) reported pitchstone with a green perlitic groundmass and idiomorphic feldspars zoned from orthoclase cores through anorthoclase to albite or oligoclase, apparently from the base of Robertsons Mountain. He noted that these volcanic rocks were petrologically and geochemically distinct from the Tertiary Nandewar Range volcanic rocks. Hanlon (1949b, 1950) recognised rhyolite, trachyte, andesite and basalt. Manser (1960) reported the presence of olivine-bearing pitchstone, locally transitional into white fluidal ignimbrite and the presence of hornblende, muscovite, quartz and/or plagioclase in various felsic volcanic rocks. McPhie (1984b) reported an assemblage of plagioclase + K-feldspar ± quartz ± altered ferromagnesians + lithic fragments and ash.

PRESENT INVESTIGATION

Five broad compositional groups are now recognised amongst the Boggabri Volcanics: basalts, andesites, dacites, pyroxene rhyolites and biotite rhyolites. These outcrop mainly as coherent lava flows or domes or small intrusives, less commonly as ignimbrites and rarely as scoria. Minor sedimentary rocks and rare airfall tuff accompany these volcanic rocks.

These five broad compositional groups are described and further subdivided below based on conventional petrographic examination augmented by extensive Na-cobaltinitrite staining for K-feldspar, selective X-ray diffraction, whole rock geochemistry (see Geochemistry chapter) and electronprobe investigation (see Mineralogy chapter). This refined subdivision cannot be employed in mapping, because not all mappable rock units have been analysed in detail.

The discussion below largely pertains to 50 registered samples (Appendix 1) which have been analysed by bulk chemical methods (XRF, INAA) or by electronprobe or exhibit a critically important but uncommon petrogenetic feature (e.g., quartz phenocrysts). These samples are designated herein as #00 to #49 (UNE samples R68600 to R68649). Twelve of the least altered samples serve as geochemical references and are referred to

below as 'select' e.g., Select Olivine Basalt for #12, abbreviated to SOB_{12}.

BASALTS

The basalts characteristically comprise olivine and plagioclase phenocrysts ± rare augite ± rare Ti-amphibole? in a groundmass of plagioclase, pyroxene and fine- to very fine-grained opaque oxides (< 150 μm). Abundance of olivine relative to plagioclase distinguishes olivine basalts from olivine-poor basalts. All sections described are from coherent lavas.

Olivine Basalt

Olivine basalt (#12, #14, #41, #46) comprises prominent magnesian olivine + calcic plagioclase phenocrysts in a groundmass of plagioclase-opaque oxide-augite ± altered glass ± enstatite or pigeonite. Of these, #12 is least altered, and serves as a reference (Select Olivine Basalt, hereafter SOB_{12} — see Fig. 11).

Texturally, these rocks are moderately to strongly porphyritic tending to seriate, and medium-grained or medium- to fine-grained. Olivine and plagioclase phenocrysts are commonly up to 2 mm in diameter, and rarely up to 6 mm, and form about 30% of the rocks. These minerals occur as isolated crystals, or together as troctolitic glomeroporphyritic aggregates up to 5 mm in diameter. Groundmasses are intergranular or intersertal, tending to subtrachytic and are composed of plagioclase laths up to 1 mm, oxide granules typically < 100 μm and augite granules generally < 100 μm and commonly < 50 μm.

Olivine phenocrysts range from ≈300 μm to 2 mm and are generally altered to iddingsite and less commonly bowlingite, or to silica-carbonate? + limonite, or to limonite along fractures. Iddingsite patches of ≈ 100 to 200 μm are probably altered olivine microphenocrysts. In SOB_{12}, many olivine gains larger than 500 μm and some grains as small as 200 μm contains fresh, uniform patches of olivine (Fo_{84-86}) enclosed by bowlingite or iddingsite (Fig. 11). #46 contains uniform patches of less magnesian olivine (Fo_{72-77}).

Plagioclase occurs as prismatic, commonly zoned phenocrysts ranging from 500 μm to 2 mm and less commonly to 6 mm in diameter, as well as groundmass laths in ranging from <100 μm to ≈ 500 μm (typically 200 to 300 μm). The phenocrysts commonly have uniform calcic plagioclase cores (less commonly zoned cores) and thin, slightly more sodic rims. Plagioclase phenocrysts in SOB_{12} are mainly An_{67-70}, possibly ranging to An_{85}, but cores are typically An_{72} (bytownite) and rims about An_{67} (labradorite). The range in #46 is from An_{86-46}. Some phenocrysts contain subhedral to euhedral inclusions of

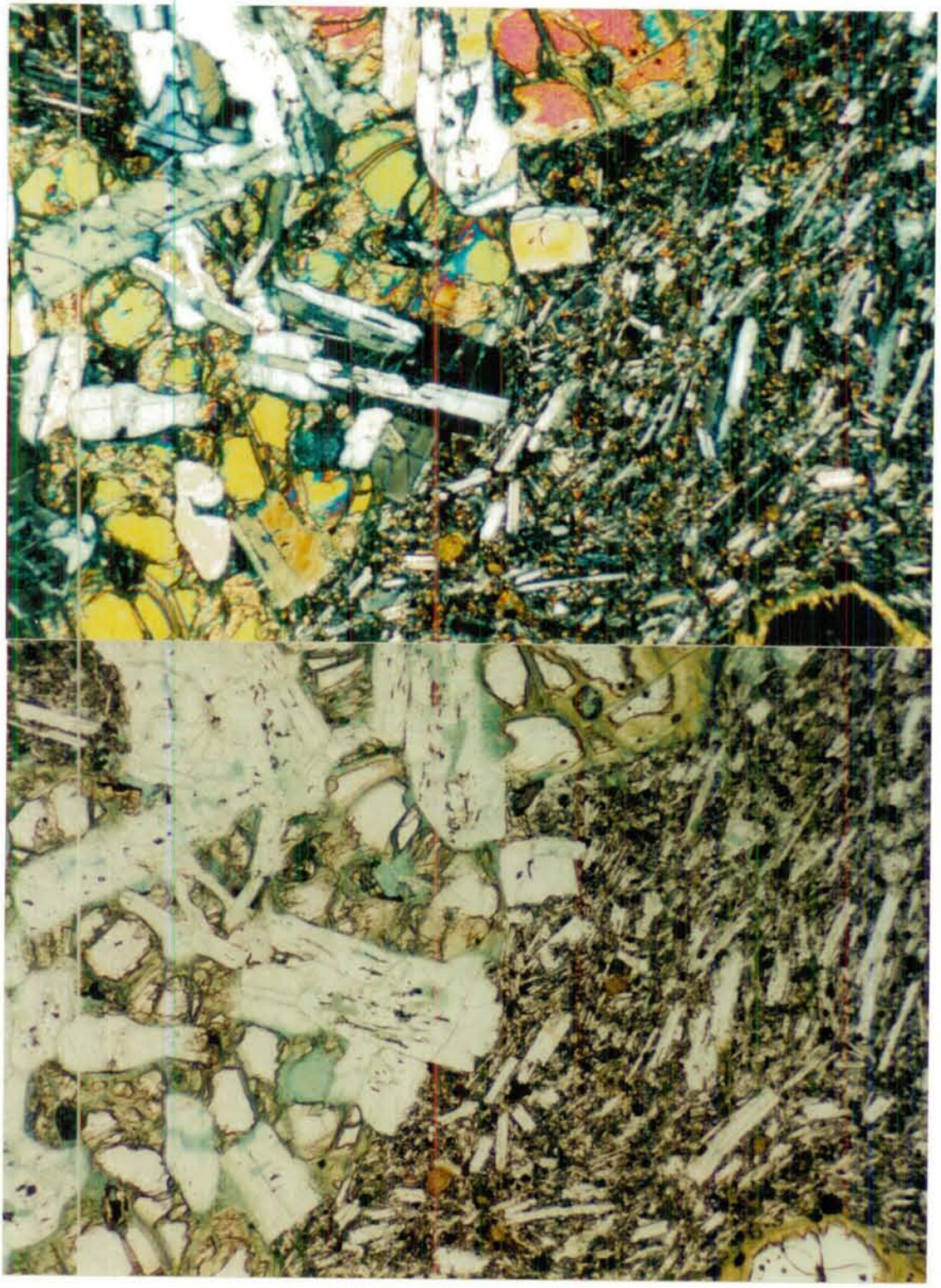

Fig. 11: Select olivine basalt (SOB_{12}) showing troctolite aggregate of forsteritic olivine-calcic plagioclase-Cr spinel in a groundmass of plagioclase-augite-opaque oxides-altered glass. (a) crossed polars; (b) plane polars. Field of view ≈3 mm x 2 mm.

augite generally less than 50 μm diameter. Chlorite alteration patches are sparsely developed.

Pyroxene is mainly restricted to the groundmass where it forms granules, although #46 contains sparse, small augite phenocrysts to 150 μm and rare subophitic augite patches to 250 μm diameter. Enstatite (En_{76}) is recorded in #46, and pigeonite is recorded as microphenocrysts (up to 100 μm) in both #46 ($En_{65}Wo_{12}Fs_{23}$) and SOB_{12} ($En_{65}Wo_6Fs_{29}$). Groundmass augite generally occurs as tiny granules (<50 μm) that average $En_{45}Wo_{40}Fs_{15}$ in SOB_{12} and $En_{47}Wo_{39}Fs_{14}$ in #46.

Oxides occur mainly in the groundmass as subhedral granules < 100 μm, ranging less commonly to 150 μm in diameter, or as inclusions up to 100 μm in olivine. Those in #46 are include ilmenite (Il_{82-90}) and both aluminian titanomagnetite and chromian titanomagnetite. Mg-Al chromite and chromian magnetite occur enclosed in olivine in SOB_{12}.

Olivine basalt is typically altered. Alteration varies from substantial replacement of olivine by iddingsite or bowlingite in SOB_{12} or replacement by limonite along fractures in #46, to complete alteration of olivine to bowlingite and of interstitial glass to chlorite in #14 and #41. Plagioclase is typically partly altered.

Olivine-poor Basalt

Plagioclase + lesser olivine phenocrysts characterise olivine-poor basalt (#03, #11, #33, #38, #39, #43 and #44), which are otherwise broadly similar to the olivine basalt. The only additional phase is rare Ti-amphibole? in #39. #39 is the least altered and is selected as representative (Select Olivine-poor Basalt, hereafter SPB_{39} — see Fig. 12). One altered basalt (#33) is exceptional due to its phenocryst abundance (≈ 35%), the presence of augite phenocrysts, and its relatively coarse fabric.

Texturally, olivine-poor basalt varies from nearly aphyric (SPB_{39}) to strongly porphyritic (#33). Phenocrysts vary from fine-grained to coarse-grained, and groundmasses from very fine-grained and are intersertal to intergranular, trachytic in some cases and less commonly, relatively coarse-grained. Grain size ranges for the different minerals are similar to those in the olivine basalts.

Olivine phenocrysts are generally sparse and fine-grained (< 1 mm), and less commonly up to 2 mm in diameter. The olivine is generally completely altered, most commonly to ferroan carbonate + silica ± limonite. Less commonly, olivine is partly altered to chlorite and iddingsite (e.g., SPB_{39}). Olivine cores in SPB_{39} averages Fo_{78} (rims are altered).

Plagioclase occurs as small equant phenocrysts or as fine- to medium-grained (up to

Fig. 12: Select olivine-poor basalt (SPB39) showing largely altered forsteritic olivine (large grains, lower centre) and small irregular patches of orangy brown Ti-amphibole? (centre and upper left) in a groundmass of plagioclase-augite-opaque oxides-altered mesostasis. Note that opaque oxide grains are very fine-grained. (a) crossed polars; (b) plane polars. Field of view ≈3 mm x 2 mm.

3 mm), elongate or less commonly subequant, subhedral to euhedral phenocrysts with calcic cores surrounded by thin (rarely broad) more sodic rims. Plagioclase in SPB_{39} ranges from An_{71-13}. Cores are strongly altered in some samples.

Pyroxenes occur mainly as groundmass granules (< 100 μm), less commonly augite occurs as microphenocrysts to 400 μm in SPB_{39} and 500 μm in #33. In SPB_{39}, groundmass enstatite averages (En_{77}), and groundmass augite averages $En_{44}Wo_{42}Fs_{14}$.

Rare Ti-amphibole? forms irregular patches up to 250 μm in diameter in SPB_{39} (Fig. 12).

Opaque oxides (ilmenite and titanomagnetite) are common as groundmass granules up to 50 μm and microphenocrysts to 150 μm (rarely 250 μm) in diameter.

Olivine (and enclosed Cr-spinel) plus plagioclase occur singly, or together as troctilitic aggregates.

Alteration is diverse amongst the basalts, and ranges from minimal in SPB_{39} to extreme in #33 (affecting all silicates except augite). Assemblages developed include: (a) chlorite replacing olivine, and calcite + chlorite replacing interstitial glass and partially replacing plagioclase (#38); (b) silica + martised magnetite? after olivine, calcite + silica after plagioclase (#43) and calcite + chlorite after interstitial glass; (c) hematite + zeolite? after olivine and zeolite after plagioclase and in cavities (#33); (d) silica + ferroan carbonate + limonite (or martised magnetite) after olivine, abundant calcite + chlorite after interstitial glass (#44); (e) limonite + silica? + carbonate after olivine, calcite after plagioclase phenocrysts and abundant calcite + limonite + silica? after interstitial glass (#03, #11); and (f) limonite + silica? + carbonate after olivine, calcite after plagioclase phenocrysts and abundant calcite + limonite + silica? after interstitial glass, green chlorite? replaces augite? (#03).

ANDESITES

The andesites characteristically comprise two pyroxenes, coarse opaque oxides (> 150 μm) and apatite accompanying calcic plagioclase. Absence of olivine, except for rare xenocrysts, distinguishes olivine-free andesite from olivine andesite. All andesite sections cited are from rocks mapped as coherent lavas.

Olivine Andesite

The only reliable (little altered) olivine andesite is #10, which is therefore representative (Select Olivine Andesite, hereafter SOA_{10} — see Fig. 13).

Texturally, the rock is moderately porphyritic with about 25% of fine- to medium-

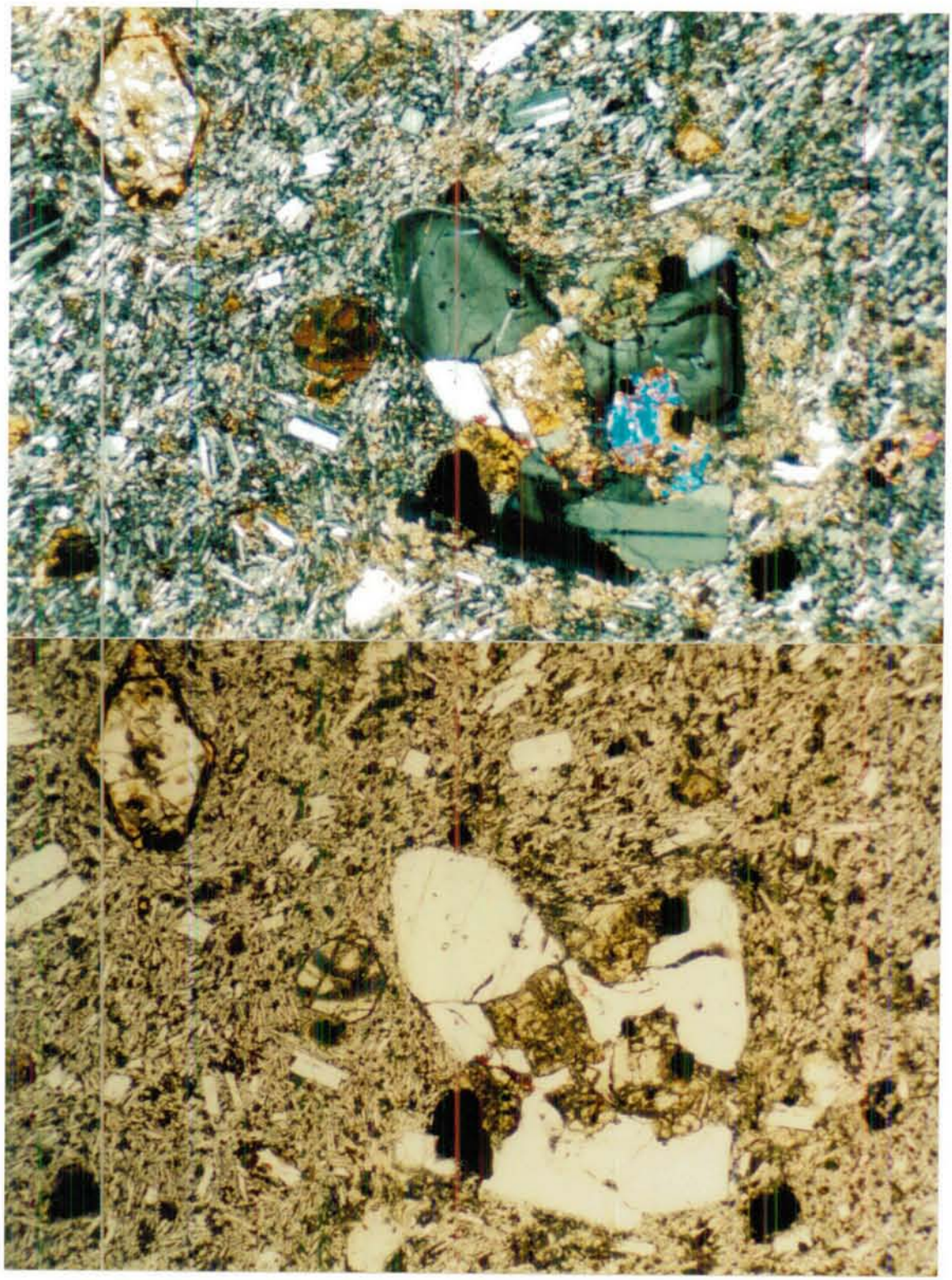

Fig. 13: Select olivine-free andesite (SOA_{10}) showing olivine (top left corner) altered to silica-ferroan carbonate and weakly limonite stained, as well as dioritic aggregates of plagioclase-clinopyroxene-altered enstatite/amphibole?-coarse opaques-coarse apatite in an atypical dacitic? groundmass. (a) crossed polars; (b) plane polars. Field of view ≈3 mm x 2 mm. Note that the augite is the most ferroan recorded.

grained phenocrysts (calcic plagioclase-opaque oxide-augite-olivine-enstatite? apatite) in a trachytic groundmass.

Olivine is subhedral, up to 1.5 mm long and altered to ferroan carbonate ± silica ± limonite.

Plagioclase is common (20%), fine- to medium-grained (up to 3 mm), elongate, commonly slightly rounded, and has broad, generally fresh cores surrounded by thin, more sodic rims. Sieve texture is common peripherally, but is rarely pervasive in calcic cores. Plagioclase also occurs in glomeroporphyritic aggregates that are up to 5 mm in diameter.

Augite phenocrysts are fresh, anhedral, commonly twinned and up to 2 mm long. The augite is the most ferroan recorded herein (see Mineralogy chapter). Ferroan carbonate pseudomorphs rounded enstatite? or amphibole? phenocrysts which are from 200 μm to 500 μm, and rarely larger.

Opaque oxides are sparse and from 150 to 400 μm in diameter. Apatite occurs as crystals up to 50 μm diameter, commonly attached to opaque oxide grains.

Augite, plagioclase, coarse oxide and coarse apatite occur singly or together as dioritic? aggregates.

Alteration is slight to moderate overall, but includes complete replacement of olivine by ferroan carbonate, silica and limonite, complete replacement of some enstatite?/amphibole? by ferroan carbonate and minor alteration of groundmass to calcite.

Olivine-free Andesite

Olivine-free andesite is characterised by the presence of two pyroxenes as phenocrysts and probably in the groundmass, relatively coarse oxide grains (>150 μm), the presence of apatite (up to 25 μm diameter) and by the absence of olivine (#09, #20, #42). However, #15 contains a single medium-grained, altered, nearly euhedral olivine surrounded by a bleached halo, and #42 is too altered and too fine-grained to establish its mineralogy reliably. #20 is also strongly altered. #09 is freshest and is chosen as representative (Select Olivine-free Andesite, hereafter SFA_{09}).

Texturally, the olivine-free andesites are diverse, ranging from nearly aphyric with sparse, fine-grained phenocrysts (#42) to strongly porphyritic with about 20% medium- and fine-grained phenocrysts (SFA_{09}). The largest phenocrysts (invariably plagioclase) range in size from about 1 mm (#42) to about 5 mm (#20). Glomeroporphyritic aggregates mainly comprising plagioclase up to 7 mm in diameter, are also sparsely developed (#20). Sparse lithic (andesitic?) fragments are also present (SFA_{09}, #15).

Groundmasses are varied and range from very fine-grained hyalopilitic with reddish brown glass (SFA_{09} and #15) to fine-grained intersertal (#20).

Plagioclase forms subhedral crystals up to 5 mm long. Many have apparently uniform to weakly zoned cores, with thin, more sodic rims. Some cores have sieve-textured peripheries, and some are skeletal with altered brown glass inclusions (cf Fig. 26 *in* McKenzie et al., 1982). Rare, strongly zoned phenocrysts are also present. Plagioclase in olivine-free andesites displays a large An range: An_{44-49} in SFA_{09}; and An_{24-52} in #15.

Clinopyroxene forms euhedral to subhedral crystals up to 1.5 mm long. These average $En_{45}Wo_{41}Fs_{14}$ in #15. Some are twinned. Orthopyroxene forms sparse anhedral to subhedral crystals up to about 1 mm long. These range from En_{74-61} in #15. A single analysis of groundmass pigeonite ($En_{63}Wo_7Fs_{30}$) is also recorded from SFA_{09}.

Opaque oxides form anhedral crystals up to 400 μm in diameter. Those in #15 and #49 comprise ilmenite in the range Il_{94-75}, and titanomagnetite in the range Usp_{23} to Usp_{73}.

Apatite occurs as very small crystals of < 25 μm in diameter, mainly grown epitaxially on oxide grains or enclosed in plagioclase or less commonly augite.

Phenocrysts and glomeroporphyritic aggregates comprise plagioclase, augite, enstatite, opaque oxides and possibly relict amphibole.

Alteration is variable. Apparently fresh glass occurs in SFA_{09} and #15, whereas #42 has chloritised pyroxene and chloritised and silicified glass, and #20 is strongly ferruginised.

DACITES

Dacites characteristically comprise one or two pyroxenes, relatively coarse oxide granules (> 250 μm) and apatite (> 25 μm in diameter and up to 750 μm in length) and ubiquitous plagioclase, but lack olivine and quartz. The presence of significant augite relative to enstatite distinguishes augite dacite (#24, #35, and probably #36 and #47) from enstatite dacite (#05, #18, #19, #26, #30, and probably #16, #17 and #40). However, alteration makes some of these assignments tentative. Dacites occur both as lavas and ignimbrites, but the dacite ignimbrites have been excluded from detailed analysis.

Augite Dacite

Two pyroxenes + coarse oxide + apatite + plagioclase characterise augite dacite. The only augite dacite with fresh glass is #24 which is therefore representative (Select Augite

Dacite, hereafter SAD_{24} — see Fig. 14).

Texturally, the augite dacite lavas are slightly to strongly porphyritic, and fine- to medium-grained. SAD_{24} contains sparse patches of brown glass in a finely recrystallised groundmass.

Plagioclase phenocrysts are common, fine- to medium-grained (up to 2.5 mm), elongate to equant, commonly subhedral. Zoning is common both as thin more sodic peripheries surrounding more calcic cores and within plagioclase cores. Plagioclase in SAD_{24} ranges from sodic andesine to bytownite (An_{34-76}), but in #47 ranges from calcic oligoclase to sodic labradorite. Some plagioclase in SAD_{24} and most in #47 is skeletal (cf Fig. 26 *in* McKenzie et al., 1982), with rounded margins and numerous large brown relict glass inclusions.

Pyroxenes are sparse, small (up to 1 mm), subhedral, and skeletal in part. Augite tends to be more common and larger than enstatite. Compositionally, enstatite in SAD_{24} forms a crude linear array ranging from En_{73-65}. Augites in SAD_{24} form a tight cluster averaging $En_{45}Wo_{41}Fs_{14}$.

Opaque oxides in augite dacite varies from rare to sparse, and from 100 μm to 400 μm, and are typically anhedral. Ilmenite is in the range Il_{81-89}, and titanomagnetite in the range Usp_{32-41}.

Enstatite Dacite

Enstatite + coarse oxide + coarse apatite + plagioclase ± minor augite phenocrysts without quartz characterises enstatite dacite (#05, #07, #16, #17, #18, #19 and #40). #05 is the freshest and is selected as representative (Select Enstatite Dacite, hereafter SED_{05} — see Fig. 15).

Textures of most enstatite dacites are coherent indicating they are lavas. The large ignimbrites of the Daisymede Domain are probably enstatite dacite, but have not been analysed in detail. Included among these are densely welded zones and black vitrophyres resembling black rhyolitic vitrophyres described below. SED_{05} is a buff coloured vitrophyre with perlitic cracking that strongly resembles the pitchstones developed among the rhyolites, but is distinguished by lower water content (see Geochemistry chapter). Enstatite dacite is sparsely to strongly porphyritic, and fine- to medium-grained. Some, including #16, contain altered glomeroporphyritic aggregates up to 8 mm in diameter.

Plagioclase is generally fine- to medium-grained (up to 3 mm), and rarely coarse, anhedral to euhedral, elongate to subequant. Peripheral sieve texture is prominent in some slides. Plagioclase in SED_{05} is fine- and less commonly medium-grained (mainly

Fig. 14: Select augite dacite (SAD_{24}) showing dioritic aggregates of plagioclase-augite-enstatite-opaques-coarse apatite with interstitial glass inclusions in a glassy dacitic groundmass. (a) crossed polars; (b) plane polars. Field of view ≈3 mm x 2 mm.

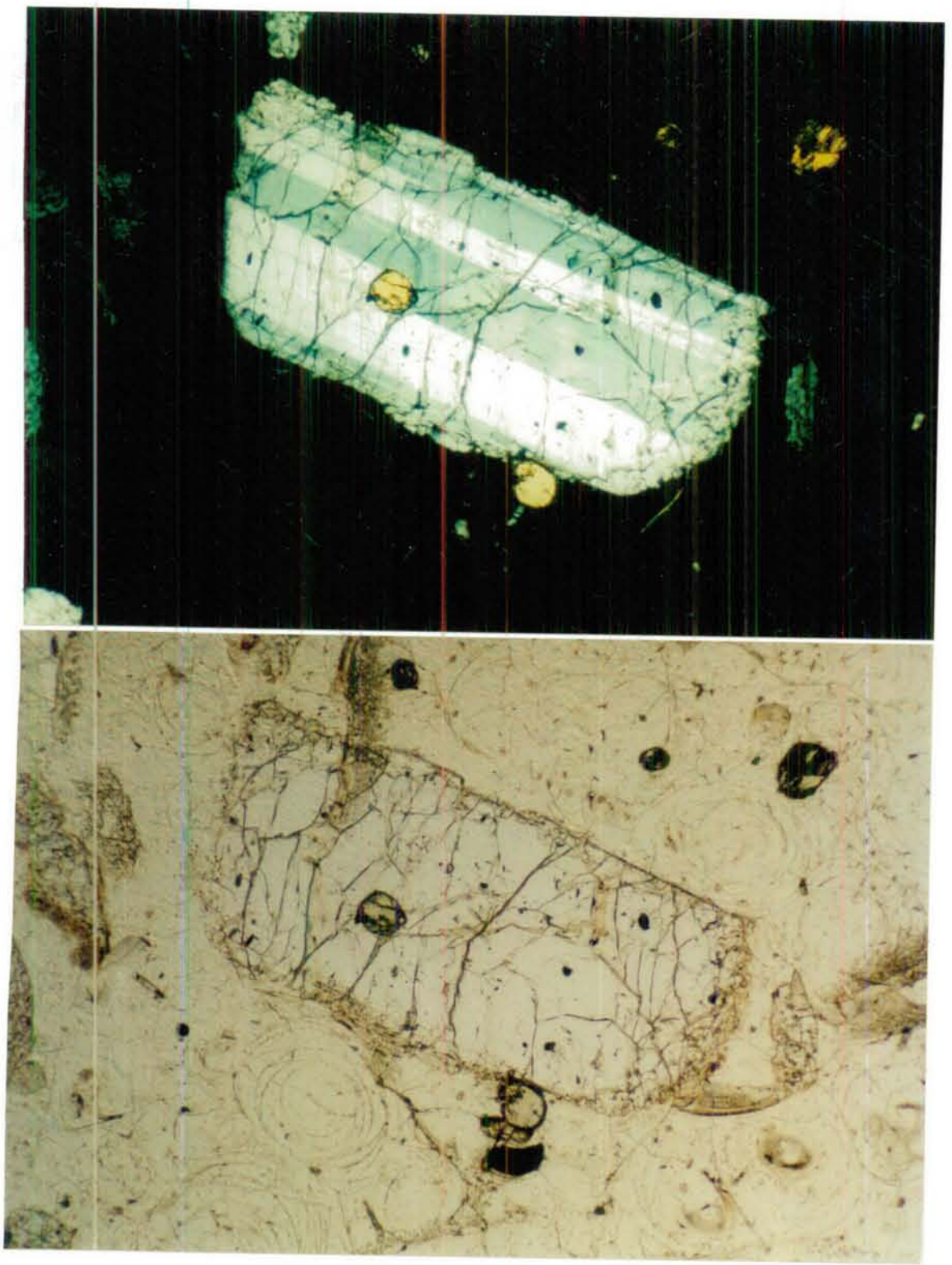

Fig. 15: Select enstatite dacite (SED_{05}) showing large slightly rounded sodic plagioclase and several small rounded enstatite grains in a perlitic groundmass. (a) crossed polars; (b) plane polars. Field of view ≈3 mm x 2 mm. Note: this rock resembles $SMPR_{06}$, but has a significant lower water content and therefore is not a pitchstone.

0.5 to 1 mm), anhedral, and rounded and contains numerous brown glass inclusions in outer sieve-textured margins that are free of sodic rims. The plagioclase is mainly calcic oligoclase (An_{22-29}) in SED_{05}.

Pyroxene is mainly small (< 1 mm) rounded, slightly elongate to equant enstatite grains. Enstatites in SED_{05} average $En_{69}Wo_3Fe_{28}$ (range En_{67-71}). Ferroan carbonate apparently pseudomorphs a second ferromagnesian (amphibole?) in #30.

Opaque oxide is sparse (very sparse in #40), fine-grained (100 to 250 μm), anhedral. Only ilmenite has been detected in SED_{05}, that being in the range Il_{73-77}. Apatite grains up to 750 μm occur in enstatite dacites and are typically associated with opaque oxides.

One dacite (#19) contains a distinctive, elongate mineral with amphibole-like cross section (oxyhornblende?) that has been replaced by limonite stain + carbonate.

Pyroxene, plagioclase, opaques and coarse apatite commonly occur singly, but also form glomeroporphyritic aggregates in some samples (e.g., #16) which contains apatite grains up to 750 μm long (see Fig. 16a).

Alteration of dacites is diverse and includes: (a) strong sericitic alteration (#16); (b) perlitic alteration in a crystal-poor pitchstone (SED_{05}); (c) coarse granophyric quartz replacing groundmass (#36); (d) green or yellow chlorite after pyroxene; (e) strong leaching (#40); (f) common groundmass silicification and development of snowflake texture; and (g) extensive calcite replacement (#07).

PYROXENE RHYOLITES

Pyroxene rhyolites characteristically comprise enstatite plus plagioclase and opaques, and lack biotite and quartz. Augite? or biotite? occur sporadically as rare tiny groundmass phases. The relative abundance of enstatite compared to plagioclase distinguishes melanocratic pyroxene rhyolite (#06) from leucocratic pyroxene rhyolite (#01, #02, #13, #22, #08, #28, #29, #31, #34, #37). Leucocratic pyroxene rhyolites with altered ferromagnesian relicts and lacking biotite are included among pyroxene rhyolites because the relicts texturally resemble enstatite rather than biotite.

Melanocratic Pyroxene Rhyolite

Prominent enstatite and a typically dark colour distinguishes melanocratic pyroxene rhyolite from leucocratic pyroxene rhyolite (except for vitrophyres which are inevitably black). Only one convincing example (#06) is available and is representative (Select Melanocratic Pyroxene Rhyolite, hereafter $SMPR_{06}$).

Texturally, $SMPR_{06}$ is a pitchstone that comprises rounded phenocrysts of

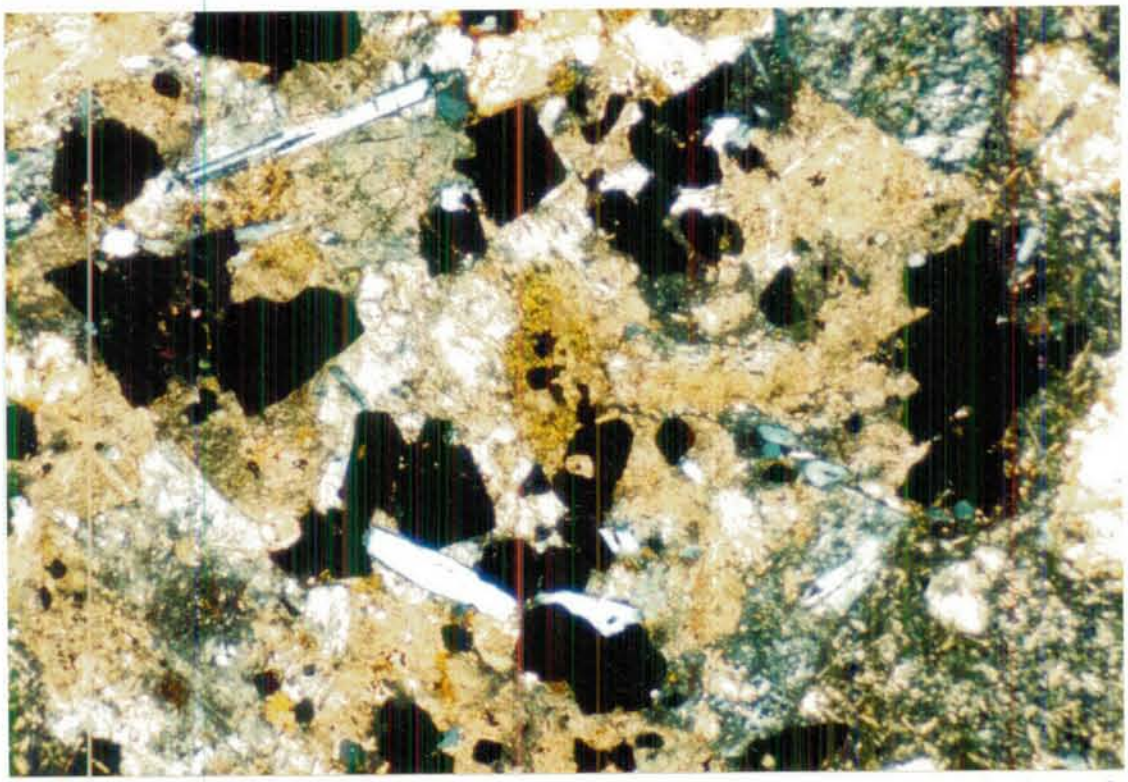

Fig. 16a: Altered augite? dacite (#16) showing dioritic aggregates of plagioclase-pyroxene-coarse opaques-coarse apatite in an altered groundmass. Note the abundance of relatively coarse apatite (white and unaltered) as equant to elongate grains up to 750 μm long (plane polars). Field of view ≈3 mm x 2 mm.

Fig. 16b: Select leucocratic pyroxene rhyolite ignimbrite ($SLPR_{13}$) showing sodic plagioclase and basaltic lithics (upper right corner) in a largely homogenised groundmass that preserves vitroclastic textures on the left hand side. Plane polars — groundmass appears black under crossed polars. Field of view ≈3 mm x 2 mm.

plagioclase, enstatite, opaque oxides, and apatite in hyalopilitic groundmass with well developed perlitic cracking and relict (nearly homogenised) vitroclastic fabric. It closely resembles SED_{05}.

Plagioclase in $SMPR_{06}$ is calcic oligoclase (An_{21-24}), and is common to sparse, fine- to medium-grained (up to 1.5 mm), very ragged to subhedral or less commonly euhedral, and commonly sieve-textured. Elongate plagioclase phenocrysts are less common.

Enstatite is the sole phenocrystic phase recorded from the pyroxene rhyolites. It occurs as small rounded crystals to 250 μm and in the range En_{66-74} in $SMPR_{06}$. Select melanocratic pyroxene rhyolite also contains tiny augite? microphenocryst recorded in the groundmass of $SMPR_{06}$ using elemental mapping (using 'new probe' described in Mineralogy chapter).

Opaque oxides in $SMPR_{06}$ are sparse, anhedral to subhedral microphenocrysts up to 150 μm in diameter. Other accessories include a trace of apatite to 100 μm in length and zircon.

Leucocratic Pyroxene Rhyolite

A phenocryst assemblage of plagioclase + opaque oxides + sparse altered enstatite phenocrysts but lacking quartz and biotite characterises leucocratic pyroxene rhyolite. #29 and #13 are the least altered lava and ignimbrite vitrophyre respectively and are representative (Select Leucocratic Pyroxene Rhyolites, hereafter $SLPR_{29}$ and $SLPR_{13}$).

Texturally, pyroxene rhyolites are mainly altered, hyalopilitic lavas with <1 to 15%, medium- to fine-grained phenocrysts in a groundmass of feldspar microlites and altered glass. Leucocratic pyroxene rhyolites also occur as texturally diverse ignimbrites, ranging from poorly-welded ignimbrites comprising ash, shards, non-flattened pumice and cognate lithics (#02) to nearly homogenised vitrophyres with only minor relicts of a former eutaxitic fabric (e.g., $SLPR_{13}$ — see Fig. 16b). Phenocryst contents are highest among the ignimbrites (up to 30%) and least amongst the lavas (range from 15% to nearly aphyric).

Plagioclase is medium- to fine-grained (up to 3 mm long), subequant, and anhedral to subhedral. Electronprobe data indicate mainly sodic oligoclase in leucocratic pyroxene rhyolite lava (An_{17-19} in $SLPR_{29}$), but a broader range in ignimbrites (An_{8-63} in $SLPR_{13}$). The latter also contains basaltic lithics.

Very sparse, subhedral to euhedral, sub-equant to slightly elongate, fine-grained (200 to 500 μm long) enstatite replaced by limonite-silica ± ferroan carbonate occur in many of the leucocratic rhyolites. The morphology of the pseudomorphs suggests that they are replacing enstatite rather than biotite, hence the identification herein.

Ilmenite appears to be the sole opaque phase. It occurs as rare, fine-grained (generally < 200 μm less commonly up to 500 μm), subhedral to anhedral grains, and exhibits an extended range from Il_{71-100} in $SLPR_{29}$. Other accessories include fine-grained apatite and zircon, commonly epitaxial on opaques, and a high relief, red-brown Ti-Al(-Ba?) silicate. In addition, $SLPR_{29}$ contains tiny biotite? microphenocryst recorded in the groundmass using elemental mapping.

Three types of alteration are manifest: white rhyolite, pitchstones, and silicified rhyolite. The first two styles affect both porphyritic lavas with relict hyalopilitic textures e.g #34, and ignimbrites with vitrified (some homogenised) eutaxitic fabrics. The third style affects lavas and less welded ignimbrite.

White rhyolite is characterised by an off-white to pale colour and chalky appearance in hand specimen. Silica (± alkali feldspar) replaces groundmass, and some feldspars and fills cavities. Fine-grained (< 100 μm) snowflake texture is extensively developed along with locally coarser patches of highly irregular, inclusion-filled quartz. Examples include #28, #34 and #37.

Pitchstones are dark green and resinous. They exhibit hackly fracture in hand specimen and perlitic fracturing of the glassy groundmass in thin section. Thin anisotropic zones mark the perlitic fractures and contrast with the adjacent isotropic glass. Plagioclase phenocrysts are commonly also fractured, and pyroxene is commonly altered. This style of alteration is developed both in porphyritic lavas with relict hyalopilitic textures (e.g., $SLPR_{29}$) and in ignimbrites with vitrified eutaxitic fabrics (e.g., $SLPR_{13}$ — see Fig. 16b).

Silicified rhyolites include very hard, pink, hematite-silica-altered rhyolites (#1 and #22), and silicified non-welded ignimbrite (#2).

BIOTITE RHYOLITES

Biotite rhyolites characteristically comprise a trace of biotite (<1%) and zircon in addition to sodic plagioclase, opaque oxides and apatite, and lack pyroxene and K-feldspar. Some biotite rhyolites also contain quartz or anorthoclase? These assemblages are present both in coherent lavas and in ignimbrites. Biotite rhyolites strongly resemble the leucocratic pyroxene rhyolites in mineralogy and petrology (apart from different ferromagnesians), lithofacies, field occurrence and alteration styles, for example, 'white rhyolite' and pitchstone.

Quartz-free Biotite Rhyolite

Biotite + plagioclase ± anorthoclase without quartz characterises quartz-free biotite

rhyolites. This sub-group is by far the more common type of biotite rhyolite (#04, #25, #32 and #48). #04 and #25 are the least altered lava pitchstone and ignimbrite vitrophyre pitchstone respectively and are representative (Select Quartz-free Biotite Rhyolites, hereafter $SFBR_{04}$ and $SFBR_{25}$).

Texturally, biotite rhyolite lavas are mainly sparsely to moderately porphyritic with < 10% phenocrysts in hyalopilitic groundmasses of feldspar microlites and altered glass. Biotite rhyolite ignimbrites are also present (e.g., $SFBR_{25}$). These display similar mineralogies and grain fabrics to the lavas, but with a greater crystal content (≈ 10%). A small proportion of the plagioclase crystals appear to be broken. Welding is variable, but sufficient in some to produce vitrophyres (e.g., $SFBR_{25}$). $SFBR_{25}$ also displays a relatively high proportion of accessories, including common apatite inclusions in plagioclase and biotite.

Feldspar in #48 comprises sodic oligoclase (range An_{14-19}, average An_{16} and Or_{3-5}, average Or_4) and anorthoclase? (range An_{8-10} and Or_{8-17}). Plagioclase is typically subhedral to anhedral, elongate to subequant, and up to 2.5 mm long. Anorthoclase has only been confirmed by electronprobe analysis in one sample (#48) where it forms small (< 0.5 mm) equant to slightly elongate crystals. Anorthoclase is apparently insensitive to the staining technique used (sodium cobaltinitrite after HF etching) and therefore could also be present in other biotite rhyolites.

Biotite in these rocks is up to 2 mm long, platy (elongate in cross section) with ragged outlines. Some is replaced by chlorite with silica occurring along the foliation.

Oxide grains range up to 500 μm in lavas and up to 750 μm in ignimbrites. Grains > 100 μm are most common, but all sizes are conspicuously sparse. Other accessories include fine-grained apatite and zircon, commonly epitaxial on opaques, and an unidentified, high relief, red-brown Ti-Al(-Ba?) silicate.

Quartz-free biotite rhyolites exhibit the same styles of alteration as leucocratic pyroxene rhyolites, with 'white rhyolite' being most common (e.g., #32 and #48) and pitchstones being less common (e.g., $SQBR_{04}$ and $SQBR_{25}$).

Quartz-Biotite Rhyolite

The quartz-biotite rhyolites are virtually identical to the biotite rhyolites except for the addition of quartz phenocrysts. The quartz forms rounded and embayed to subhedral phenocrysts to 500 μm in diameter. #00 is chosen as representative (Select Quartz-Biotite Rhyolite, hereafter $SQBR_{00}$ — see Fig. 17). Quartz-biotite rhyolite exhibits 'white rhyolite' alteration, or less commonly, spectacular spherulites (#00).

Fig. 17: Quartz-biotite rhyolite (#00) showing rounded, unzoned quartz (grey in right centre), euhedral, zoned sodic plagioclase (grey in centre), euhedral, fresh, fine-grained biotite (left centre) and opaques with attached zircon and apatite in a spherulitic groundmass. (a) crossed polars; (b) plane polars. Field of view ≈3 mm x 2 mm.

SUMMARY

Fig. 18 illustrates the occurrence of phenocrysts in the ten compositional types recognised herein. The essential characteristics of the Boggabri Volcanics are as follows:

1. A range of compositions from olivine basalt to biotite rhyolite and pyroxene rhyolite.
2. Ubiquitous plagioclase throughout the suite.
3. A phenocryst assemblage of (Cr-spinel)-olivine-plagioclase (troctolite) in basalts occurring as isolated crystals and as glomeroporphyritic aggregates.
4. Olivine in all basalts, and in olivine andesite.
5. No olivine in more felsic rocks apart from a single altered xenocryst in one andesite (#15).
6. Augite phenocrysts in some olivine-poor basalts and apparently throughout the andesite-augite dacite range, and groundmass augite in basalts and possibly in $SMPR_{06}$.
7. Ti-amphibole? in SPB_{39}.
8. Enstatite or altered enstatite apparently throughout the andesite-dacite range and in most (all?) rhyolites lacking biotite; this range broadly overlaps that of augite in the andesite-augite dacite range.
9. Pigeonite/enstatite as a groundmass phase in some basalts, and pigeonite as a groundmass phase in at least one andesite.
10. Restricted development of amphibole, including small Ti-amphibole? phenocrysts in SPB_{39}, probable altered amphibole? phenocrysts in #19 (dacite), and possible altered amphibole phenocrysts in SOA_{10} and #30 (enstatite dacite).
11. A hybrid assemblage in SOA_{10}, including olivine (typical of basalts) and coarse oxide-apatite-evolved augite (indicative of dacite) accompanying plagioclase.
12. Notably coarser opaque oxides in the andesite-dacite range than in basalts.
13. Ubiquitous apatite in the andesite-dacite-rhyolite range with dacites and SOA_{10} containing notably coarser apatite.
14. Biotite in some rhyolites.
15. No phenocryst assemblages comprising biotite-enstatite or augite-enstatite in rhyolites, but possible occurrence of enstatite accompanied by rare groundmass biotite in $SLPR_{29}$ and by groundmass augite in $SMPR_{06}$.
16. Identified phenocrystic quartz in only a few biotite rhyolites (secondary quartz is present in some other rocks).
17. No recognised K-spar and very limited anorthoclase (in biotite rhyolites).
18. Zircon in all? rhyolites, but not in dacites (#40 excepted).
19. An unidentified Ti-Al(-Ba?) silicate in some rhyolites.

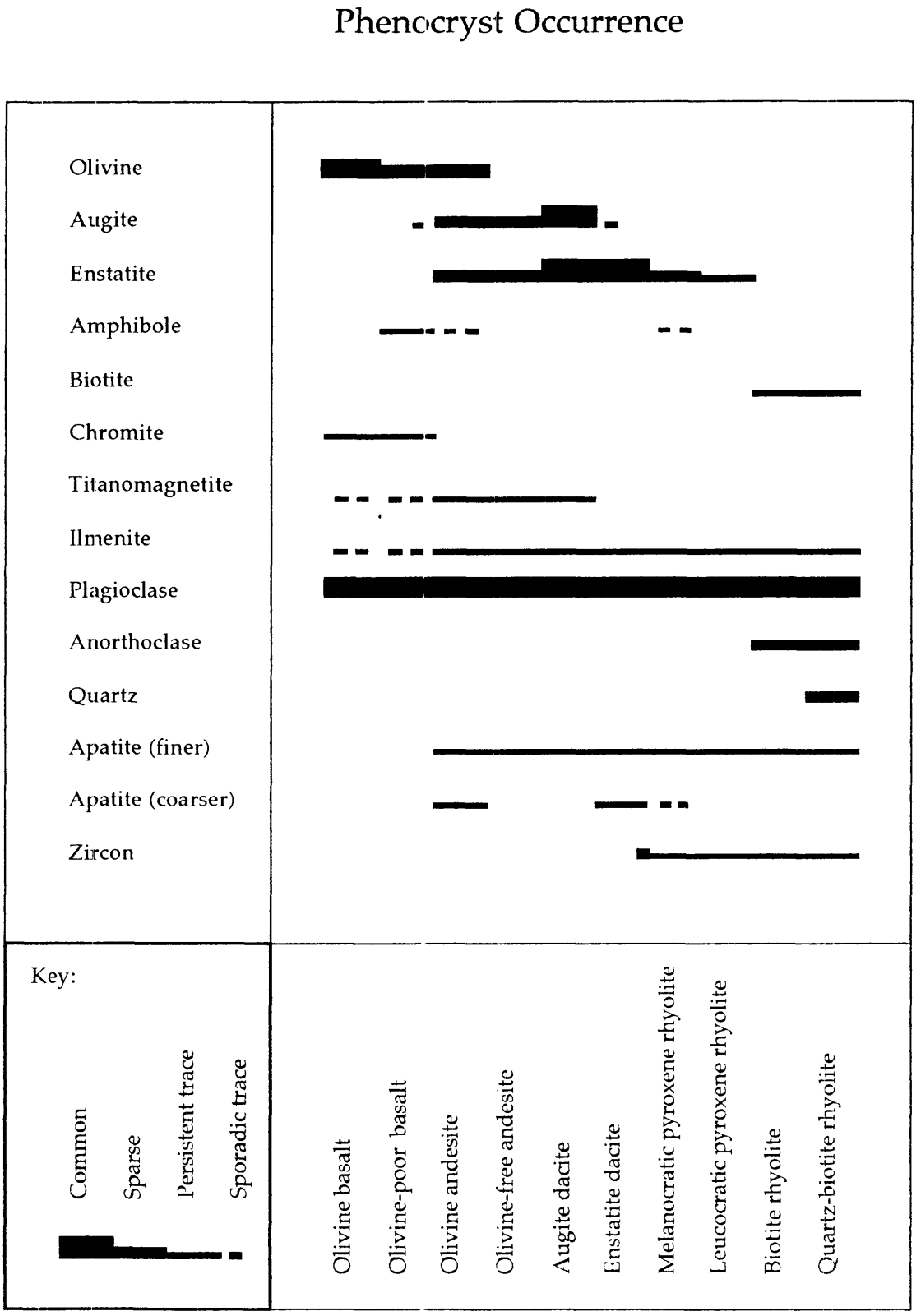

Fig. 18: Compositional control on phenocryst occurrence in Boggabri Volcanics — see text for explanation.

20. Fresh glass in two olivine-free andesite (SFA_{09} and #15) and one augite dacite (SAD_{24}).
21. Fresh but hydrated glass inclusions in plagioclase in some rhyolites and dacites.
22. Development of welding fabrics ranging from negligible to extreme, including vitrification (forming vitrophyres) and rarely, homogenisation of glass destroying vitroclastic fabrics (e.g., $SLPR_{13}$).
23. Common conversion of rhyolite lava to pitchstone containing perlitic texture.
24. Less common conversion of rhyolitic ignimbrite vitrophyre to pitchstone containing perlitic texture.
25. Uncommon development of perlite texture in dacite (e.g., SED_{05}).

Petrographic observations herein confirm Jenson's (1907) report of pitchstone with perlitic cracking and distinct petrographic differences from the Tertiary Nandewar volcanics (based on descriptions by Stolz, 1983); a compositional range from rhyolite to basalt (Hanlon 1949b, 1950); and the presence of ignimbrites (Manser, 1960; McPhie, 1984b). However, the following are **not** corroborated:

- 'idiomorphic feldspars zoned from orthoclase cores through anorthoclase to albite or oligoclase' (Jensen, 1907): an extremely unusual zoning which is probably misidentified;
- olivine-bearing pitchstone, locally transitional into white fluidal ignimbrite (Manser (1960): rhyolites lack olivine, but some contain enstatite, and a **biotite** rhyolite ignimbrite at Robertsons Mountain ($SFBR_{25}$) displays a transition from white, foliated rock to pitchstone;
- the presence of hornblende, muscovite, quartz and/or plagioclase in various felsic volcanic rocks (Manser, 1960): relict amphibole is uncommon, quartz is rare in Boggabri Volcanics and muscovite is rare among rhyolites internationally (Deer, Howie and Zussman, 1992); and
- an assemblage of plagioclase + K-feldspar ± quartz ± altered ferromagnesians + lithic fragments and ash (McPhie, 1984b): K-spar has not been observed, and the only mappable rock units recognised with phenocrystic quartz are biotite rhyolites in the Daisymede section of McPhie (1984b).

PETROGRAPHIC COMPARISONS

The ubiquitous presence of plagioclase and generally regular appearance or disappearance of major phases suggests broad petrographic coherence. Principal anomalies include: (a) SOA_{10} with a hybrid assemblage of olivine (basaltic affinity) and evolved augite plus relatively coarse apatite (dacitic affinity); (b) the presence of two discrete leucocratic rhyolite assemblages (biotite- and pyroxene-bearing types); and (c)

the presence of Ti-amphibole? in one basalt.

Petrology indicates a sub-alkaline affinity through the coexistence of two or three pyroxenes in andesites, most dacites and the groundmasses of some basalts (BVSP, 1981; Wilson, 1989), but Ti-amphibole? in the groundmass of SPB_{39} indicates a tendency to mild alkalinity. The troctolitic phenocryst assemblage and aggregates in SOB_{12} are typical of MORB, but are more primitive than in most continental suites and atypical of arcs or OITs where early clinopyroxene (i.e. preceding or accompanying plagioclase respectively) would be expected (BVSP, 1981; Wilson, 1989). Similarly, the lack of enstatite phenocrysts in basalt indicates a MORB rather than arc or OIT affinity. The lack of olivine in most andesites, dacites and rhyolites or Fe-enrichment in pyroxenes generally, distinguishes Boggabri Volcanics from some evolved MORB and CFB suites (BVSP, 1981; Wilson, 1989). The apparent rarity of amphibole and restricted occurrence of quartz and biotite is atypical of arc volcanic rocks and the lack of pigeonite as a pyroxene phase among more felsic rocks is compatible with MORB affinity (Wilson, 1989). The apparent absence of K-spar is typical of arc tholeiites or low-K calc-alkaline volcanic rocks (BVSP, 1981; Wilson, 1989).

Regional comparisons based on literature data indicate close similarity to the Werrie Basalt (Vickers, 1991, 1993) and probably (based on sparse published data) to the Warrigundi Igneous Complex in the Werrie Basin (Flood et al., 1988) and the basal volcanic rocks in the Gunnedah Basin (Leitch, 1993). However, the Werrie Basalt and especially the Warrigundi Igneous Complex could be marginally more alkaline.

Chapter 4: Mineralogy

INTRODUCTION

This investigation represents the first study of the chemical composition of the minerals in the Boggabri Volcanics. It is mainly based on electron microprobe investigations carried out in two stages at the Electron Microscope Unit at UNE.

The bulk of the probe work was carried out in 1992–93 using a JEOL JSM–35 scanning electron microscope fitted with a Tracor-Northern EDS detector, a Canberra S100 analyser and 'SPEED' software (designed by N.G. Ware, of Research School of Earth Sciences, ANU). Analytical configuration comprised an accelerating voltage of 15 kV, a beam current of 1 nA, a beam size of 1 μm and 100 s real time counting. The results are referred herein as 'old probe analyses'. These analyses were reputedly reliable, apart from some reservations concerning feldspars (N.D.J. Cook, P. Garlick, pers. comm., 1992).

Supplementary analyses were carried out in 1996. This was to fill gaps in data that arose partly from quality control problems with the earlier work, and partly from a shift of emphasis in sample selection, following completion of geochemical interpretation. This work employed a new facility at UNE (the 'new probe') encompassing a JEOL JSM–5800LV scanning electron microscope fitted with a Link ISIS microanalysis system (Oxford Instruments) comprising a Pentafet Super ATW EDS detector and ISIS software. These analyses were carried out using default conditions (typical detector resolution about 100 eV). Analytical configuration comprised an accelerating voltage of 20 kV, a beam current of 1 nA, a beam size of 1 μm and 100 s real time counting.

Subsequently, extensive testing (in conjunction with P. Garlick, Manager of the Electron Microscope Unit, UNE, and with advice from J. Sheffield-Parker, Manager Oxford Instruments Microanalysis Systems) established optimum acquisition conditions (including detector resolution about 65 eV), and significantly improved calibration over that available from built-in (default or 'virtual') standards for most major elements. The supplementary analyses were then reprocessed. Stringent quality controls were developed and applied as part of this process, eliminating all of the supplementary feldspar data, a few supplementary olivine and pyroxene analyses, as well as a few more

of the old probe data. Limited available time permitted reanalysis of only a few additional data under optimum acquisition conditions. At the time of writing, Na and minor element calibrations for the new probe required further refinement, so 'new probe' results are reported herein as indicative analyses, subject to case-by-case assessment.

Fe^{3+}/Fe^{2+} calculations herein use SPEED software for old probe data and the method of Droop (1987) for new probe data.

Professor R.L Stanton kindly carried out some additional analyses on $SLPR_{29}$ (leucocratic pyroxene rhyolite pitchstone) at the Research School of Earth Sciences (ANU — operated by N.G. Ware). These are designated as 'ANU probe' analyses, and were carried out using a WDS detector.

OLIVINE

Table 2 and Fig. 19 summarise the mineral chemistry of olivine from basalts (SOB_{12}, SPB_{39} and #46). Petrologically the latter is an olivine basalt, but was not analysed by XRF owing to the lack of a suitable sample. Olivine in more felsic rocks is rare and is always altered.

Acceptance criteria for olivine analyses (for 4 oxygens — cf Deer, Howie and Zussman, 1992; Brown, 1982) are: (a) Σcations = 2 ± 0.02 (i.e. ± 1%); (b) Si = 1 ± 0.01 (i.e. ± 1%); and (c) ΣM^{2+}/ Si = 2.00 ± 0.04 (i.e. ± 2%), where ΣM^{2+} is the sum of divalent cations (Mg^{2+}, Ca^{2+}, Mn^{2+} and Fe^{2+}). These criteria eliminated only a few analyses by either old or new probes. Acceptable old probe data yield the following results: (a) Σcations average 2.00 (range 1.99 to 2.01, n=6) for SOB_{12} and 2.00 (range 1.99 to 2.02, n=17) for #46; Si averages 1.00 (range 1.00 to 1.01) for SOB_{12} and 1.00 (range 0.99 to 1.01) for #46; ΣM^{2+}/ Si averages 2.00 (range 1.98 to 2.02) for SOB_{12} and 2.01 (range 1.98 to 2.04) for #46. Acceptable new probe data yield: (a) Σcations averaging 1.99 (n=1) for SOB_{12} and 2.00 (range 1.99 to 2.01) for SPB_{39}; (b) Si averaging 1 for SOB_{12} and 2.00 (range 1.99 to 2.01, n=9) for SPB_{39}; (c) and ΣM^{2+}/ Si averaging 1.99 for SOB_{12} and 2.01 (range 1.99 to 2.02) for SPB_{39}. These data are acceptable despite poor detector resolution. This probably because the wide gaps between the Ka peaks for Mg (1.24 eV), Si (1.74 eV) and Fe (6.4 eV) allows successful discrimination between peaks even at 100 eV resolution, and because peak broadening at low resolution does not necessarily result in significant relative reduction in peak area (the basis of quantitative analysis — Reed, 1996) for these elements.

Graphical data presentation and classification herein largely follows Deer, Howie and Zussman (1992) and Brown (1982).

Table 2: Average Olivine Analyses and Calculated Parameters

	SOB12	*SOB12*	*#46*	*SFB39*
Probe	new	old	old	new
Rock*	ob	ob	ob	pb
No. of analyses	n=1	n=6	n=17	n=9
Oxides				
SiO_2	39.90	39.95	38.15	38.63
FeO*	14.80	14.47	23.36	20.33
MnO	0.24	0.19	0.27	0.47
MgO	44.50	45.52	38.20	40.25
CaO	0.19	0.00	0.00	0.20
NiO	0.33	0.21	0.28	0.12
Total	99.96	100.33	100.00	100.00
Cations				
Si	1.00	1.00	1.00	1.00
Fe^{2+}	0.31	0.30	0.51	0.44
Mn	0.00	0.00	0.01	0.01
Mg	1.67	1.70	1.49	1.55
Ca	0.00	na	na	0.01
Ni	0.01	0.00	0.00	0.00
Total	2.99	3.00	3.00	3.00
Parameters				
$\Sigma M2+$	1.99	2.00	2.01	2.00
$\Sigma M2+/Si$	1.99	2.00	2.01	2.01
Fo	84	85	75	78

* All Fe as FeO; ob = olivine basalt; pb = olivine-poor basalt; na = not available

$\Sigma M2+$ = sum of divalent cations ($Mg^{2+} + Fe^{2+} + Mn^{2+} + Ca^{2+} + Ni^{2+}$)

$\Sigma M2+/Si$ = the ratio of divalent cations to silica

$Fo = Mg^{2+}/(Mg^{2+} + Fe^{2+} + Mn^{2+})$

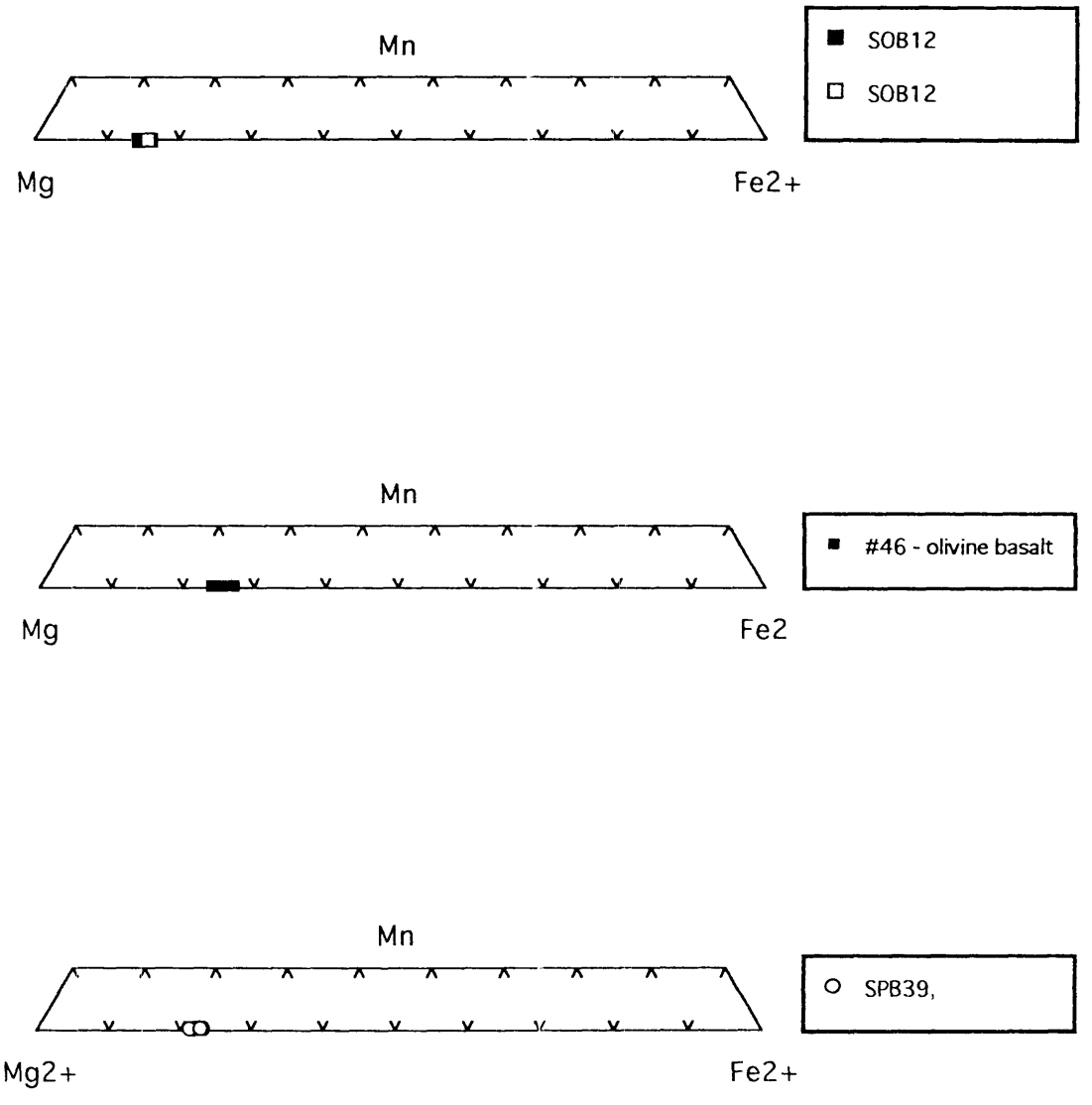

Fig. 19: Olivine compositions in olivine basalt and olivine-poor basalt. Note: open symbols indicate new probe data, closed symbols indicate old probe data — see text for explanation.

Basalts

Old probe analyses of olivine in SOB_{12} are in the range Fo_{84-86} (average Fo_{85}, n = 6). The limited range is consistent with the petrographic uniformity of the olivine cores (rims are altered). New probe data for SOB_{12} amount to a single analysis of Fo_{84} (which is within the old probe range).

Only new probe analyses of olivine are available for SPB_{39}. These are in the range Fo_{77-79} (average Fo_{78}, N = 9). Rims are all altered. Cores display minimal variation, consistent with petrographic uniformity.

Old probe data for olivine in #46 (unanalysed olivine basalt) are in the range Fo_{72-77} (average Fo_{74}). These values are significantly less than SOB_{12}, despite the petrographic similarity. Some analyses overlap the lower range of SPB_{39}.

All analyses display negligible contents of Ca, Mn and Ni (all values ≤ 0.01 cation per 4 oxygens). Those from the new probe are regarded as semi-quantitative only owing to incomplete calibration, but are virtually identical to those from the old probe.

Summary

New and old probes yielded acceptable results in three narrow ranges between Fo_{86} and Fo_{72}.

PYROXENES

Table 3 and Fig. 20 summarise mineral chemistry for pyroxene from twelve samples using the old probe and ten samples using the new probe. These samples span the range from olivine basalt to melanocratic pyroxene rhyolite. Three unanalysed rocks, one olivine basalt (#46), one andesite (#49) and one dacite (#47) are included for comparison.

Acceptance criterion for pyroxene analyses is (for 6 oxygens, after Morimoto, 1988; and Deer, Howie and Zussman, 1992): Σcations = 4 ± 0.04 for 6 oxygens (i.e. ± 1%). Applying more stringent quality control criteria would require independent determination of the structural assignment of Al (4 or 6-fold sites) and the oxidation state of iron. Many new analyses appear to be acceptable for major elements, for similar reasons to olivine: wide gaps between the peaks for Mg, Si and Fe, as well as that for Ca (3.69 eV) apparently allows successful discrimination between peaks, and because peak broadening at low resolution (e.g., Mg) does not necessarily result in significant relative reduction in peak area. However, minor elements occurring between these peaks are probably less well discriminated and their analyses are regarded as semi-quantitative pending further testing. Therefore, only old probe data is used for minor element plots.

Table 3a: Average Old Probe Pyroxene Compositions and Calculated Parameters

	#46	*#49*	*#15*	*#47*	*#24*	*#46*
Rock	ob	an	an	dc	dc	ob
Mineral	aug	aug	aug	aug	aug	pig
No. of analyses	n = 5	n = 1	n = 15	n = 10	n = 5	n = 1
Oxides						
SiO_2	51.21	52.31	51.34	50.89	51.95	52.61
TiO_2	1.05	0.26	0.66	0.67	0.50	0.45
Al_2O_3	2.06	1.02	2.36	2.39	1.90	1.60
FeO*	9.13	8.87	9.58	9.54	8.86	15.00
MnO	0.34	0.55	0.40	0.37	0.36	0.53
MgO	16.43	15.76	15.84	15.31	15.93	23.87
CaO	19.37	20.85	19.50	20.53	20.25	5.94
Na_2O	0.41	0.38	0.32	0.31	0.25	0.00
Total	100.00	100.00	100.00	100.00	100.00	100.00
Cations						
Si	1.90	1.94	1.90	1.91	1.93	1.92
Ti	0.03	0.01	0.02	0.02	0.01	0.01
Al	0.09	0.05	0.10	0.11	0.08	0.07
Fe3+	0.10	0.10	0.09	0.07	0.05	0.07
Fe2+	0.19	0.18	0.21	0.23	0.22	0.39
Mn	0.01	0.02	0.01	0.01	0.01	0.02
Mg	0.91	0.87	0.87	0.85	0.88	1.30
Ca	0.77	0.83	0.77	0.82	0.81	0.23
Na	0.03	0.03	0.02	0.02	0.01	0.00
Cation Total	4.00	4.00	4.00	4.01	4.00	4.00
Parameters						
FeOt	0.26	0.27	0.28	0.27	0.26	0.45
Al IV	0.09	0.05	0.09	0.10	0.07	0.07
Al VI	0.00	0.00	0.01	0.01	0.01	0.00
Fe^{3+} IV	0.01	0.02	0.00	0.00	0.00	0.01
Fe^{3+} VI	0.07	0.08	0.09	0.05	0.04	0.06
Mg#	0.83	0.83	0.81	0.79	0.80	0.77
En	0.47	0.44	0.45	0.44	0.45	0.65
Wo	0.39	0.42	0.40	0.42	0.41	0.12

Rock types: ob = olivine basalt; an = andesite; dc = dacite; rp = pyroxene rhyolite

Minerals: aug = augite; en = enstatite; pig = pigeonite

* FeOt is Fe reported as FeO; Fe^{3+} calculated by method of Droop (1987); 4- and 6-fold co-ordination of Al and Fe^{3+} (Al IV, Al VI, Fe^{3+} IV and Fe^{3+} VI) after Morimoto (1988);

Mg# = $Mg^{2+}/(Mg^{2+} + Fe^{2+} + Mn^{2+})$; En = $Mg^{2+}/(Mg^{2+} + Fe^{2+} + Mn^{2+} + Ca^{2+})$

Wo = $Ca^{2+}/(Mg^{2+} + Fe^{2+} + Mn^{2+} + Ca^{2+})$

Table 3a: Average Old Probe Pryoxene Compositions and Calculated Parameters (Cont.)

	#46	*#15*	*#47*	*#24*	*#05*	*#06*
Rock	ob	an	dc	dc	dc	rp
Mineral	en	en	en	en	en	en
No. of analyses	n = 1	n = 8	n = 21	n = 27	n = 13	n = 48
Oxides						
SiO_2	53.5	52.67	53.53	53.39	53.58	53.33
TiO_2	0.83	0.24	0.18	0.27	0.00	0.15
Al_2O_3	0.99	1.28	1.01	1.21	0.88	0.74
FeO*	14.25	18.92	17.31	16.74	18.29	19.14
MnO	0.40	0.69	0.93	0.68	1.66	1.61
MgO	28.58	24.58	25.88	26.19	24.46	23.92
CaO	1.45	1.38	1.16	1.33	0.92	0.88
Na_2O	0.00	0.24	0.00	0.20	0.21	0.24
Total	100.00	100.00	100.00	100.00	100.00	100.00
Cations						
Si	1.93	1.95	1.95	1.94	1.97	1.98
Ti	0.02	0.01	0.01	0.01	0.00	0.00
Al	0.04	0.06	0.04	0.05	0.04	0.03
Fe3+	0.00	0.04	0.05	0.05	0.03	0.04
Fe2+	0.43	0.54	0.48	0.45	0.53	0.55
Mn	0.01	0.02	0.03	0.02	0.05	0.05
Mg	1.54	1.36	1.41	1.42	1.34	1.33
Ca	0.06	0.06	0.04	0.05	0.04	0.03
Na	0.00	0.02	0.00	0.02	0.02	0.02
Cation Total	4.03	4.01	4.00	4.00	4.00	4.00
Parameters						
FeOt	0.43	0.55	0.52	0.50	0.55	0.57
Al IV	0.04	0.04	0.04	0.05	0.02	0.02
Al VI	0.00	0.01	0.00	0.00	0.01	0.02
Fe3 + IV	0.00	0.00	0.01	0.01	0.00	0.00
Fe3 + VI	0.00	0.01	0.04	0.04	0.02	0.01
Mg#	0.78	0.71	0.75	0.76	0.71	0.71
En	0.76	0.69	0.71	0.72	0.69	0.69
Wo	0.03	0.03	0.02	0.03	0.02	0.02

Rock types: ob = olivine basalt; an = andesite; dc = dacite; rp = pyroxene rhyolite

Minerals: aug = augite; en = enstatite; pig = pigeonite

* FeOt is Fe reported as FeO; Fe^{3+} calculated by method of Droop (1987); 4- and 6-fold co-ordination of Al and Fe^{3+} (Al IV, Al VI, Fe^{3+} IV and Fe^{3+} VI) after Morimoto (1988);

Mg# = $Mg^{2+}/(Mg^{2+} + Fe^{2+} + Mn^{2+})$; En = $Mg^{2+}/(Mg^{2+} + Fe^{2+} + Mn^{2+} + Ca^{2+})$

Wo = $Ca^{2+}/(Mg^{2+} + Fe^{2+} + Mn^{2+} + Ca^{2+})$

Table 3b: Average New Probe Pyroxene Compositions and Calculated Parameters

	SOB12	*SPB39*	*SOA10*	*SFA09*	*SOB12*
Rock	ob	bs	oa	an	ob
Mineral	cpx	cpx	cpx	cpx	pig
No. of analyses	n = 5	n = 9	n = 26	n = 9	n = 2
Oxides					
SiO_2	51.86	51.60	52.24	52.49	53.54
TiO_2	0.53	0.84	0.32	0.48	0.19
Al_2O_3	1.50	1.57	0.38	1.00	1.16
Cr_2O_3	0.28	0.05	0.00	0.08	0.03
FeO*	9.60	8.81	12.44	8.88	18.44
MnO	0.28	0.27	0.52	0.34	0.53
MgO	15.94	15.63	14.63	16.20	23.11
CaO	19.94	20.98	19.21	20.21	2.84
Na_2O	0.07	0.25	0.27	0.32	0.17
Total	100.00	100.00	100.00	100.00	100.01
Cations					
Si	1.93	1.92	1.97	1.95	1.97
Ti	0.02	0.02	0.01	0.01	0.01
Al	0.06	0.07	0.02	0.04	0.05
Cr	0.01	0.00	0.00	0.00	0.00
Fe	0.30	0.27	0.39	0.28	0.57
Mn	0.01	0.01	0.02	0.01	0.02
Mg	0.88	0.87	0.82	0.90	1.27
Ca	0.80	0.84	0.78	0.80	0.12
Na	0.00	0.02	0.02	0.02	0.01
Cation Total	4.01	4.02	4.03	4.01	4.02
Parameters					
Mg#	0.75	0.76	0.68	0.76	0.69
En	0.45	0.44	0.41	0.45	0.65
Wo	0.40	0.42	0.39	0.41	0.06

Rock types: ob = olivine basalt; an = andesite; dc = dacite; rp = pyroxene rhyolite

Minerals: aug = augite; en = enstatite; pig = pigeonite

* FeOt is Fe reported as FeO; Fe^{3+} calculated by method of Droop (1987); 4- and 6-fold co-ordination of Al and Fe^{3+} (Al IV, Al VI, Fe^{3+} IV and Fe^{3+} VI) after Morimoto (1988);

Mg# = $Mg^{2+}/(Mg^{2+} + Fe^{2+} + Mn^{2+})$; En = $Mg^{2+}/(Mg^{2+} + Fe^{2+} + Mn^{2+} + Ca^{2+})$

Wo = $Ca^{2+}/(Mg^{2+} + Fe^{2+} + Mn^{2+} + Ca^{2+})$

Table 3b: Average New Probe Pyroxene Compositions and Calculated Parameters (Cont.)

	SOB09	*SPB39*	*SFA09*	*SED05*	*SMPR06*
Rock	an	bs	an	dc	rp
Mineral	pig	opx	opx	opx	opx
No. of analyses	n = 1	n = 1	n = 8	n = 9	n = 4
Oxides					
SiO_2	53.00	55.57	53.91	53.90	53.62
TiO_2	0.28	0.00	0.19	0.08	0.14
Al_2O_3	0.17	1.28	0.22	0.00	0.00
Cr_2O_3	0.11	0.00	0.04	0.00	0.00
FeO*	19.39	14.96	16.19	18.86	19.07
MnO	0.78	0.08	0.58	2.24	1.85
MgO	22.66	27.93	26.86	23.98	24.19
CaO	3.28	0.18	1.68	0.95	0.99
Na_2O	0.32	0.00	0.32	0.16	0.16
Total	99.99	100.00	99.99	100.16	100.02
Cations					
Si	1.97	1.99	1.96	1.99	1.98
Ti	0.01	0.00	0.00	0.00	0.00
Al	0.01	0.05	0.01	0.00	0.00
Cr	0.00	0.00	0.00	0.00	0.00
Fe	0.60	0.45	0.50	0.58	0.59
Mn	0.03	0.00	0.02	0.07	0.06
Mg	1.26	1.49	1.46	1.32	1.34
Ca	0.13	0.01	0.06	0.04	0.04
Na	0.02	0.00	0.02	0.01	0.01
Cation Total	4.03	3.99	4.03	4.01	4.02
Parameters					
Mg#	0.68	0.77	0.75	0.69	0.69
En	0.63	0.77	0.73	0.68	0.68
Wo	0.07	0.00	0.03	0.02	0.02

Rock types: ob = olivine basalt; an = andesite; dc = dacite; rp = pyroxene rhyolite

Minerals: aug = augite; en = enstatite; pig = pigeonite

* FeOt is Fe reported as FeO; $Fe3^+$ calculated by method of Droop (1987); 4- and 6-fold co-ordination of Al and Fe^{3+} (Al IV, Al VI, $Fe3^+$ IV and $Fe3^+$ VI) after Morimoto (1988);

Mg# = $Mg^{2+}/(Mg^{2+} + Fe^{2+} + Mn^{2+})$; En = $Mg^{2+}/(Mg^{2+} + Fe^{2+} + Mn^{2+} + Ca^{2+})$

Wo = $Ca^{2+}/(Mg^{2+} + Fe^{2+} + Mn^{2+} + Ca^{2+})$

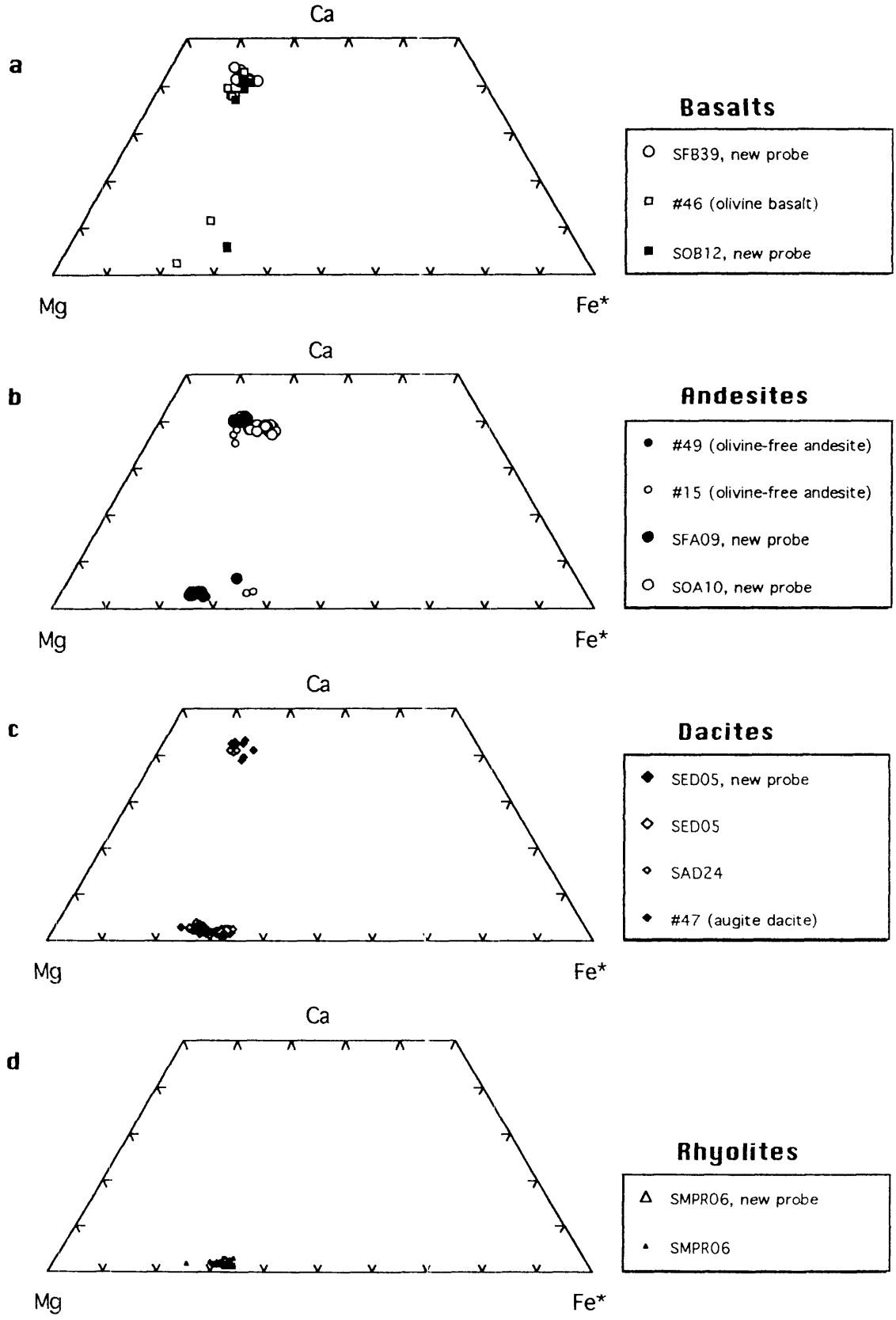

Fig. 20 (a–d): Pyroxenes form the Boggabri Volcanics. (a–d) pyroxene quadrilateral. Data by old probe except where indicated. See text for explanation.

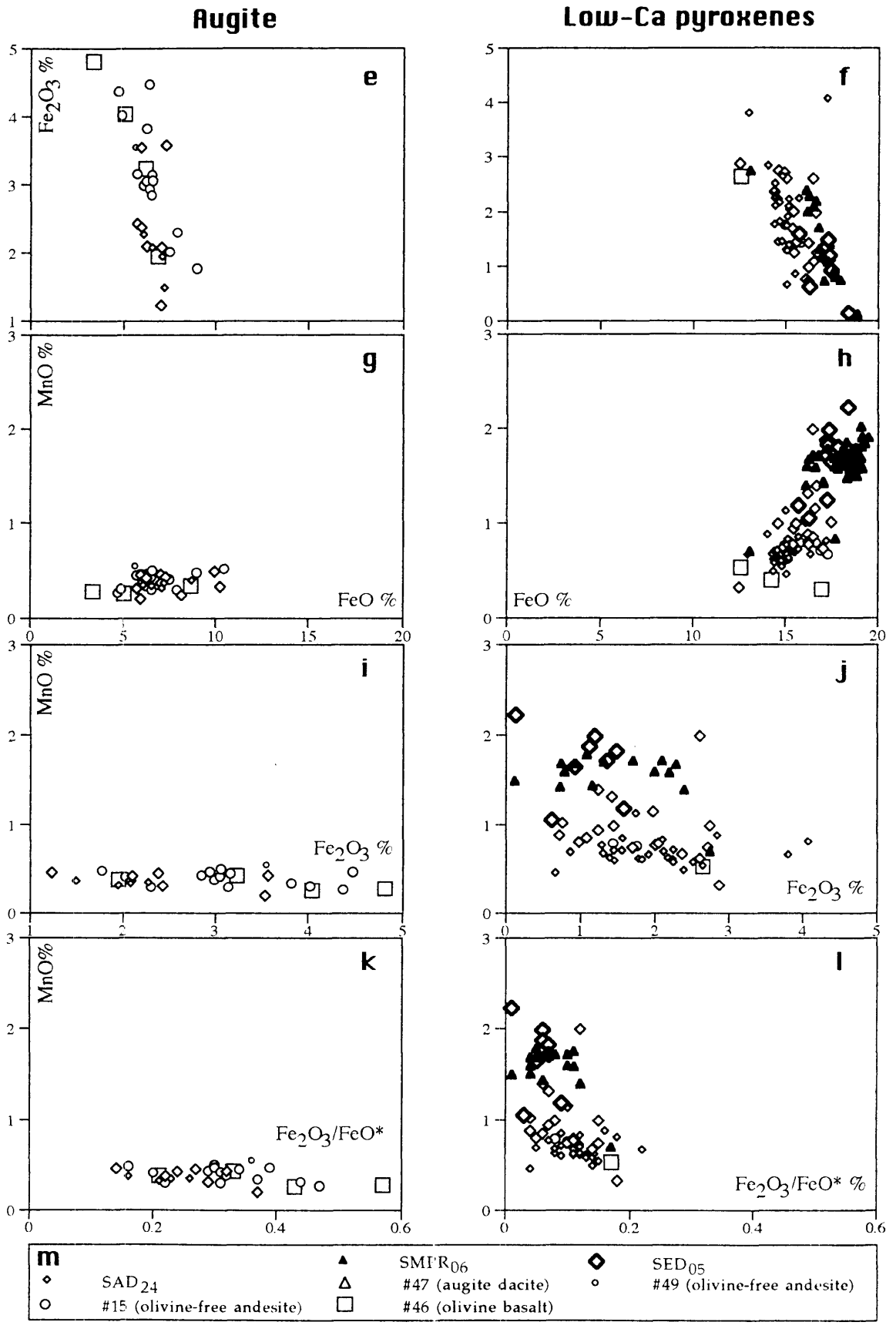

Fig. 20 (e–l): Pyroxenes cont. — Fe oxidation state and MnO contents. All data by old probe. FeO* = FeO + Fe_2O_3 + MnO. See text for explanation and Fig. 20 (m) for symbols.

In addition, Droop's (1987) method and SPEED software produce slightly different Fe^{3+}/Fe^{2+} assignments for some analyses (most noticeable among the most reduced augites). This discrepancy has not been fully investigated, so for consistency only old probe data are used for where iron oxidation state is important.

Graphical data presentation and classification herein largely follows Morimoto (1988) and Deer, Howie and Zussman (1992).

Overview

Two remarkably restricted pyroxene compositions dominate the Boggabri Volcanics: enstatite in the range En_{61-77} (average En_{70}) and Wo_{0-4} (average Wo_2), and augite in the range to En_{40-49} (average En_{44}) and Wo_{36-44} (average Wo_{40}). The former occur in the basalt-augite dacite range, whereas the latter are rare in enstatite dacite and melanocratic pyroxene rhyolite but are abundant in more mafic rocks. In addition, pigeonite has been tentatively identified in the groundmass of olivine basalt and andesite.

Basalts

Low-Ca pyroxenes exhibiting a limited compositional range occur in the groundmasses of basalts. One enstatite ($En_{76}Wo_3Fs_{21}$) is recorded from an olivine basalt (#46 — old probe data). Slightly more ferroan enstatite (average $En_{77}Wo_0Fs_{23}$) occurs in SPB_{39} (new probe data). Pigeonite occurs in SOB_{12} (two analyses, average $En_{65}Wo_6Fs_{29}$ — new probe) and in #46 (average $En_{65}Wo_{12}Fs_{23}$ — old probe).

Augite clusters more tightly for all compositions. The augite in olivine basalt averages $En_{45}Wo_{40}Fs_{15}$ in SOB_{12} (new probe), and $En_{47}Wo_{39}Fs_{14}$ in #46 (old probe), whereas that in SPB_{39} averages $En_{44}Wo_{42}Fs_{14}$ (new probe). Augite in basalts is thus marginally less calcic than that in olivine-poor basalt, and data from the old and new probe overlap.

Andesites

Andesites (SFA_{09}, #15, #49) exhibit a tight clustering of enstatite data, one pigeonite analysis, and tightly clustered augite data. In contrast, SOA_{10} yields a distinctly more iron-rich set of augite data.

Enstatite in one andesite (#15, old probe) forms a restricted linear array in the range En_{61-72} at about Wo_3 (old probe). Those in SFA_{09} are similar (average $En_{73}Wo_3Fs_{26}$ — new probe). A single analysis of groundmass pigeonite ($En_{63}Wo_7Fs_{30}$ — new probe) is also recorded from SFA_{09}.

Augite in olivine-free andesite has a similar composition to that in basalt, forming a

loose cluster around $En_{45}Wo_{41}Fs_{14}$. However, augite in SOA_{10} is anomalous, being slightly but distinctly more iron-rich than all other augites.

Dacites

Augite dacite (SAD_{24}, #47) contains both enstatite and augite, whereas SED_{05} contains only enstatite phenocrysts.

Enstatite in augite dacite forms a crude linear array in the range En_{65-73} (average $En_{72}Wo_3Fs_{25}$ — old probe).

Enstatite in SED_{05} averages $En_{69}Wo_2Fe_{29}$ (range En_{68-71} — old probe), and $En_{68}Wo_2Fs_{30}$ (range En_{67-69}) by the new probe. Thus old and new probe analyses are virtually identical for SED_{05}, and also overlap the more felsic part of the range in SAD_{24}. Furthermore, the enstatite compositional range in dacites overlaps that of andesites.

Augite in SAD_{24} forms a tight cluster averaging $En_{45}Wo_{41}Fs_{14}$ (range En_{45-46}, Wo_{41-42} — old probe). This average is identical to that in the andesites cited above.

Rhyolites

Only enstatite phenocrysts are recorded from $SMPR_{06}$, which is the only analysed melanocratic pyroxene rhyolite. However, tiny augite? microphenocrysts were recorded in the groundmass of $SMPR_{06}$ using elemental mapping on the new probe.

The enstatite in $SMPR_{06}$ averages $En_{69}Wo_2Fs_{29}$ (range En_{66-74} — old probe) and $En_{68}Wo_2Fs_{30}$ (range En_{68-69} — new probe). These ranges overlap and extend to only slightly more ferrosilite-rich compositions than those present in dacites.

Minor Components

MnO values and iron oxidation state further distinguish low-Ca pyroxenes from augite (see Fig. 20e–l). This is in addition to significant differences in total iron content (5–10% in augite, 12 to 20% in low-Ca pyroxene) that are implicit in the distinction of augite from low-Ca pyroxene.

Moderate to relatively high Fe^{3+} (typically 2–5%) characterises augite whereas low to moderate Fe^{3+} (up to 3%) characterises low-Ca pyroxenes. On **Fe_2O_3 v FeO**, augite and low-Ca pyroxenes exhibit similarly steep, but distinct, negative trends. These trends are slightly flatter than that for oxidation at constant Fe. Fe^{3+} values do not distinguish individual rock types, but **Fe_2O_3 v FeO**, does poorly through higher total iron in orthopyroxenes in felsic rocks.

Low MnO (typically ≈ 0.4%) characterises augite whereas low-Ca pyroxenes are generally in the range 0.4 to 2.5%. MnO values are highest for $SMPR_{06}$ and SED_{05}, and lowest for #46 (olivine basalt). **MnO v FeO** displays a nearly flat trend for augite, whereas low-Ca pyroxenes display a steep increase in MnO with increasing FeO. **MnO v Fe_2O_3** exhibits nearly flat trends, again indicating that factors other than bulk composition control Fe^{3+}/Fe^{2+}.

$Fe_2O_3/FeO+Fe_2O_3+MnO$ is low (<0.2) in low-Ca pyroxenes, whereas augite exhibits a higher range (mainly 0.2 to 0.5). Compositional distinction is again poor, although values in augite are relatively high in #46 (olivine basalt) and low in SAD_{24}.

Al^{VI} is consistently low to zero in old probe data from both augite and low-Ca pyroxenes. Some analyses require minor Fe^{3+} in Z (four-fold co-ordinated) sites to compensate for Al^{IV} deficiency (after Morimoto, 1988).

Summary

New and old probes yield acceptable analyses of enstatite in the rock range from olivine basalt to pyroxene rhyolite, augite in the rock range from olivine basalt to augite dacite and rare pigeonite from basalts and andesites. A very restricted range of pyroxene compositions exists in bulk compositions ranging from basalt to rhyolite. MnO is significantly enriched in enstatite from more felsic rocks, whereas Fe^{3+}/Fe^{2+} is apparently independent of host rock composition. Minor Fe^{3+} occurs in Z (four-fold) sites in some pyroxenes and Al^{VI} is consistently low to zero in others. SOA_{10} is notable for containing the most iron-rich augite despite the presence of altered olivine.

FELDSPARS

Table 4 and Fig. 21 summarise mineral chemistry for feldspars from 11 samples across the Boggabri Volcanics rock range from olivine basalt to rhyolite. BaO and SrO values are not discussed as they are low by both old and new probes.

Acceptance criteria for feldspar analyses (cf Deer, Howie and Zussman, 1992; Ribbe, 1983) are as follows (assuming 8 oxygens): Σcations = 5 ± 0.05 (i.e. ± 1%); (b) framework cations (Al + Si + Fe^{3+}) = 4 ± 0.04 (i.e. ± 1%); (c) bridging cations Na+K+Ca ≈ 1 ± 0.02; (d) ratio of bridging to framework cations = 0.25 ± 0.01 (± 0.04%); and (e) Al-Ca-1 — 0.01 to +0.05. Setting criteria slightly broader than 1% for criteria (b), (c) and (d) provides some allowance for the possible occurrence of Fe^{2+} as a bridging cation in place of Fe^{3+} as a framework cation in plagioclase (cf Smith, 1983). The greater range and asymmetry in the last criterion reflects the common slight excess of Al over Ca in plagioclase in the literature (N.C.N. Stephenson pers. comm., 1996). By these criteria, old

Table 4: Average Old Probe Feldspar Compositions and Calculated Parameters

	SOB12	*#46*	*#15*	*#49*	*#47*	*SAD24*
Rock	ob	ob	an	an	dc	dc
Mineral	pl	pl	pl	pl	pl	pl
No. of analyses	n = 6	n = 24	n = 50	n = 29	n = 18	n = 64
Oxides						
SiO_2	49.66	51.27	54.72	55.26	56.42	54.92
Al_2O_3	31.99	30.63	28.25	28.15	27.46	28.43
Fe_2O_3*	0.48	0.81	0.78	0.51	0.35	0.48
CaO	14.52	12.87	10.26	9.90	9.04	10.16
Na_2O	3.12	3.99	5.55	5.69	6.16	5.57
K_2O	0.20	0.40	0.42	0.41	0.54	0.37
Total	100.00	100.00	100.00	100.00	100.00	100.00
Cations						
Si	2.27	2.34	2.47	2.49	2.54	2.48
Al	1.72	1.65	1.51	1.50	1.46	1.51
Fe^{3+}	0.02	0.03	0.03	0.03	0.02	0.02
Ca	0.71	0.63	0.50	0.48	0.44	0.49
Na	0.28	0.35	0.49	0.50	0.54	0.49
K	0.01	0.02	0.02	0.02	0.03	0.02
Cation Total	5.02	5.02	5.02	5.02	5.02	5.02
Parameters						
ΣF	4.02	4.01	4.01	4.02	4.01	4.02
ΣM	1.00	1.00	1.01	1.00	1.00	1.00
$\Sigma M/\Sigma F$	0.25	0.25	0.25	0.25	0.25	0.25
Al-Ca-1	0.01	0.02	0.01	0.02	0.02	0.02
Components						
An average	0.72	0.64	0.50	0.49	0.45	0.50
An min	0.67	0.44	0.24	0.31	0.27	0.34
An max	0.85	0.86	0.66	0.74	0.58	0.76
Or	0.01	0.02	0.02	0.02	0.03	0.02

Rock types: ob = olivine basalt; an = andesite; dc = dacite; rp = melanocratic pyroxene rhyolite; rh = leucocratic pyroxene rhyolite; rb = biotite rhyolite

Minerals : pl = plagioclase; ao = anorthoclase;

Phases: An = anorthite; Or = orthoclase

* Fe reported as Fe_2O_3

ΣF = sum of framework forming cations ($Si + Al + Fe3^+$)

ΣM = sum of bridging cations ($Na^+ + K^+ + Ca^{2+}$)

Table 4: Average Old Probe Feldspar Compositions and Calculated Parameters (Cont.)

	SED05	*SMPR06*	*SLPR13*	*SLPR29*	*#48*	*#48*
Rock	dc	rp	rh	rh	rb	rb
Mineral	pl	pl	pl	pl	pl	ao
No. of analyses	n = 11	n = 17	n = 3	n = 15	n = 8	n = 4
Oxides						
SiO_2	61.25	61.11	65.50	62.63	63.45	65.20
Al_2O_3	24.28	24.28	21.30	23.47	22.95	21.42
Fe_2O_3*	0.24	0.26	0.16	0.13	0.19	0.27
CaO	5.06	5.32	1.65	4.01	3.37	1.71
Na_2O	8.21	8.03	10.02	8.78	9.39	9.41
K_2O	0.94	0.95	1.26	0.99	0.77	2.03
Total	100.00	100.00	100.00	100.00	100.00	100.00
Cations						
Si	2.73	2.72	2.89	2.78	2.81	2.89
Al	1.27	1.28	1.11	1.23	1.20	1.12
Fe3+	0.01	0.01	0.01	0.00	0.00	0.00
Ca	0.24	0.25	0.08	0.19	0.16	0.08
Na	0.71	0.69	0.86	0.76	0.81	0.81
K	0.05	0.05	0.07	0.06	0.04	0.12
Cation Total	5.02	5.01	5.02	5.01	5.02	5.01
Parameters						
ΣF	4.01	4.01	4.00	4.01	4.01	4.01
ΣM	1.00	1.00	1.01	1.00	1.01	1.00
$\Sigma M/\Sigma F$	0.25	0.25	0.08	0.25	0.25	0.25
Ca-Al-1	0.03	0.02	0.03	0.04	0.04	0.04
Components						
An average	0.25	0.27	0.08	0.20	0.16	0.09
An min	0.22	0.21	0.08	0.17	0.14	0.08
An max	0.23	0.24	0.09	0.19	0.19	0.10
Or	0.05	0.05	0.07	0.06	0.04	0.11

Rock types: ob = olivine basalt; an = andesite; dc = dacite; rp = melanocratic pyroxene rhyolite; rh = leucocratic pyroxene rhyolite; rb = biotite rhyolite

Phases: An = anorthite; Or = orthoclase

* Fe reported as Fe_2O_3

ΣF = sum of framework forming cations ($Si + Al + Fe3^+$)

ΣM = sum of bridging cations ($Na^+ + K^+ + Ca^{2+}$)

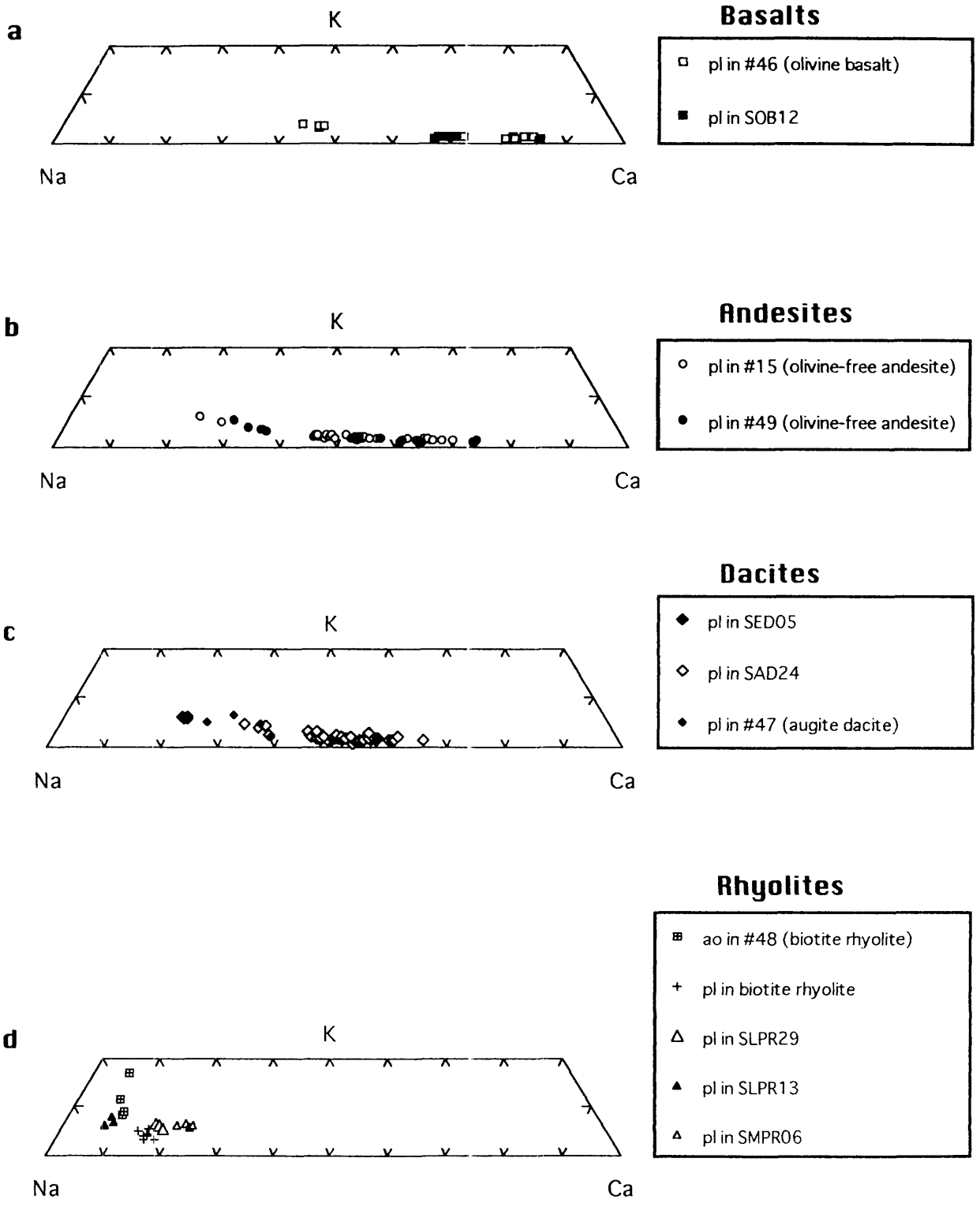

Fig. 21: Composition of feldspars in the Boggabri Volcanics. Mineral key: pl = plagioclase; ao = anorthoclase.

probe analyses are acceptable but new probe data are unacceptable. For example all old probe feldspars contain on average 4.01 framework cations (range 4.00 to 4.03), 1 bridging cation (range 0.98 to 1.02), and have a ratio or bridging cations to framework cations of 0.25 (range 0.24 to 0.26). However, supplementary new probe data are unacceptable because of a slightly high framework cation totals (ranges up to 4.06), low bridging cation total (average 0.88, range 0.75 to 0.96) and low bridging to framework cation total (average 0.22, range 0.18 to 0.24).

Poor fit indices (a 'figure of merit' for comparing peak shapes — Statham, 1996) for sodium using the new probe could be the cause of unacceptable analyses. Such poor fit could reflect the decreasing sensitivity of EDS probes with decreasing atomic number (affecting Na and lighter elements). However, Na (1.04 eV) is not necessarily the whole problem, because the energy separation from Al (at 1.49 eV) is identical to that between Mg and Si which appear to be acceptably discriminated in olivine and pyroxene. An alternative explanation is that at the low detector resolution used (≈ 100 eV), the detector cannot adequately discriminate between overlapping Al (1.49 eV) and Si (1.74 eV) peaks, leading to inaccurately assessed peak-to background values and hence incorrectly interpreted elemental abundances. A further possible problem (J. Sheffield-Parker pers. comm.) is 'pile-up' in the EDS detector whereby two nearly synchronous, low energy photons are counted as a single photon (e.g., an oxygen at 520 eV and an Na at 1.04 keV combined to produce a 1.56 keV pulse which would be counted as an Al photon at 1.49 keV), causing erroneous results. An attempt to correct Na in new probe analyses of plagioclases to meet criterion (d) (most analyses would then satisfy all criteria) produced results that were unacceptably sodic by comparison with old probe data and petrographic observations. Moreover, most uncorrected new probe plagioclase compositions fell within the range of old probe data, despite being rejected by the criteria above. Consequently, the only feldspar data reported herein are old probe data.

Graphical data presentation and classification herein largely follows Smith (1974) and Deer Howie and Zussman (1992).

Overview

Feldspar analysed by the old probe is mainly plagioclase in the range An_{86-8} except for a few anorthoclase grains tentatively identified in SFBR04. Many rocks display moderate to large An ranges. In contrast, Or values and ranges are generally very low, especially at high An values but increase with decreasing An. Plagioclase, especially large crystals, commonly displays complex internal zoning, with both normal and reverse zoning recorded. There does not appear to be any simple relationship between compositional range and crystal shape.

Basalts

Plagioclase in olivine basalt and olivine-poor basalt displays the highest An values. The An range is: An_{67-70} (with a possible range to An_{85} in some old and new probe analyses that marginally failed acceptance criteria); and An_{46-86} in olivine basalt #46.

Andesites

Plagioclase in some andesites displays an extended An range: An_{24-52} in #15 and An_{31-74} in #49. In contrast, plagioclase in #23 (mugearite from unassigned volcanics) is typically more sodic at An_{24-33}.

Dacites

Plagioclase in augite dacite also displays an extended range — An_{27-58} in #47; and An_{34-76} in SAD_{24}. In contrast, plagioclase in SED_{05} displays a limited range — An_{22-23}.

Rhyolites

Plagioclase in rhyolites generally display only limited An range. The An range in $SMPR_{06}$ is An_{21-24}, whereas that in leucocratic pyroxene rhyolite is: An_{8-9} and one value of An_{63} in $SLPR_{13}$ (the rock is an ignimbrite with basaltic lithics) and Or_{6-8}; and An_{17-19}, Or_6 in $SLPR_{29}$. $SFBR_{04}$ exhibits a range from An_{14-19} and Or_{3-5} (average 4), and also contains a distinctly more potassic group of analyses (possible anorthoclase — An_{8-10} and Or_{8-17}).

Summary

Feldspar analyses comprise plagioclase in the range from calcic bytownite to albite, as well as rare anorthoclase. The An content of the plagioclase and of the calcic limit of the plagioclase ranges broadly decrease with increasing silica content of the host rock. However, very wide compositional range (up to 40% An) is typical of most basalt, andesite and augite dacite analyses. Narrower An ranges are typical of basalts (possibly due to limited sampling) and also of enstatite dacite and melanocratic pyroxene rhyolite. In addition, Or values and ranges are generally very low, especially at high An values but increase with decreasing An. The highest values are in a discrete cluster of anorthoclase analyses in $SFBR_{04}$, and slightly lower Or contents occur in plagioclase in $SLPR_{13}$ which straddles the nominal boundary between the albite and anorthoclase fields. Some albite grains in #48 (biotite rhyolite) have distinctly lower Or contents than the general trend.

Overall, the extensive feldspar compositional range is in marked contrast to the restricted pyroxene range.

OXIDES

Table 5 and Fig. 22 summarise mineral chemistry for opaque oxides from 11 samples in the range from olivine basalt to biotite rhyolite. Several unanalysed rocks are included for comparison, including one olivine basalt (#46), one andesite (#49), one dacite (#47) and one biotite rhyolite (#48).

No *a priori* acceptance criteria are applied to opaque oxide analyses because independent assessment of Fe^{3+}/Fe^{2+} ratios is not feasible and calculation of Fe^{3+} from stoichiometry significantly changes most parameters listed in Table 5.

Generally only old probe data are used for plots of oxides because of insufficient testing of new probe data, and discrepancies between Droop's (1987) method and SPEED software noted above in assigning Fe^{3+}/Fe^{2+} in pyroxenes. New probe data are only presented for spinels from SOB_{12} (the most primitive rock), because of the need to constrain early Cr fractionation.

Graphical data presentation and classification herein largely follows Haggerty (1976), apart from some minor amendments to the spinel prism. Haggerty used a factor of 2*Ti along with Cr and Al as components of the front and back faces of the spinel prism, but used Ti in x-y plots of the prism sides. This is inconsistent and 2*Ti is used herein throughout. In addition, the spinel prism used by Haggerty (1976) lists ulvospinel and magnetite as alternative components in the classification, but the two components were plotted separately in the plotting examples. The procedure herein is to combine the two components (i.e. $2*Ti + Fe^{3+}$) as one component in the spinel prism. This component corresponds to the ulvospinel component in magnetite-ulvospinel series, and an identical calculation yields the ilmenite component in ilmenite-hematite series. The relative importance of $2*Ti + Fe^{3+}$ compared to Al+Cr, and of Ti and Fe^{3+} in spinels are indicted herein in additional diagrams not used by Haggerty (1976). Fig. 22a–b contains a legend for subsequent X-Y and triangular diagrams.

Overview

Two restricted opaque oxide compositions dominate the Boggabri Volcanics: iron-rich ilmenite and compositionally diverse titanomagnetites. Ilmenite occurs in most Boggabri Volcanics examined, and is the sole opaque oxide analysed in rhyolites. Titanomagnetite dominates mafic rocks and are recorded from olivine basalt through to augite dacite. In addition, Mg-Al-chromite grains occur enclosed in olivine from SOB_{12}.

Table 5: Average Oxide Compositions, Cation Assignments and Parameters

	SOB12	*SOB12*	*SOB12*	*SOB12*	*#46*	*#46*
Mineral	cr	cr-mt	mt	al-mt	cr-mt	mt
Rock	ob	ob	ob	ob	ob	ob
Probe	new	new	new	old	old	old
No. of analyses	n = 21	n = 2	n = 3	n = 3	n = 4	n = 9
Oxides						
TiO_2	3.19	12.16	22.16	11.81	1.78	6.91
Al_2O_3	29.12	11.09	2.17	20.66	4.69	3.35
Cr_2O_3	25.39	17.36	3.44	0.17	18.87	2.02
V_2O_3	0.25	0.35	1.14	0.55	0.00	0.63
FeO*	30.12	53.31	68.82	58.10	68.51	82.48
MnO	0.14	0.20	0.15	0.41	2.09	0.46
MgO	11.74	5.51	2.11	8.30	4.07	3.77
ZnO	0.04	0.03	0.01	0.00	0.00	0.38
Total	100.00	100.00	100.00	100.00	100.00	100.00
Cations						
Ti	0.07	0.31	0.60	0.32	0.05	0.20
Al	1.03	0.44	0.09	0.86	0.21	0.15
Cr	0.60	0.46	0.10	0.00	0.56	0.05
V	0.01	0.01	0.03	0.01	0.00	0.01
Fe3+	0.22	0.48	0.58	0.66	1.14	1.39
Fe2+	0.54	1.03	1.48	0.70	0.76	0.97
Mn	0.00	0.01	0.00	0.01	0.07	0.02
Mg	0.52	0.28	0.11	0.44	0.23	0.21
Zn	0.00	0.00	0.00	0.00	0.00	0.00
Cation Total	2.99	3.02	2.99	3.00	3.02	3.00
Parameters						
Fe2+/(Mg+Fe2+)	0.51	0.79	0.93	0.62	0.77	0.82
Cr/(Cr+Al)	0.37	0.52	0.49	0.00	0.73	0.23
(Al+Cr)/(Al+Cr+2* Ti+Fe3+)	0.82	0.46	0.10	0.41	0.60	0.59
Fe3+/(Al+Cr+Fe3+)	0.12	0.35	0.75	0.40	0.38	0.10
2*Ti/(2*Ti+Al+Cr)	0.08	0.41	0.86	0.49	0.08	0.22
2Ti/(2Ti+Fe3+)	0.40	0.57	0.67	0.43	0.11	0.67

Rock types: ob = olivine basalt; an = andesite; dc = dacite; rh = rhyolite; rb = biotite rhyolite

Minerals: cr = chromite; cr–mt = chromian magnetite; al–mt = aluminian chromite; mt = titanomagnetite; il = ilmenite

* Fe reported as FeO

Table 5: Average Oxide Compositions, Cation Assignments and Parameters (Cont.)

	#49	*#15*	*#47*	*SAD24*	*#46*	*#49*	*#15*
Mineral	mt	mt	mt	mt	il	il	il
Rock	an	an	an	dc	ob	an	an
Probe	old	old	old	old	old	old	old
No of analyses	n = 5	n = 11	n = 7	n = 22	n = 4	n = 6	n = 9
Oxides							
TiO_2	8.79	19.24	10.18	12.38	45.31	40.73	49.19
Al_2O_3	3.22	2.89	2.55	2.53	0.90	0.46	0.53
Cr_2O_3	0.00	0.00	0.19	0.00	0.20	0.00	0.00
V_2O_3	0.65	0.49	0.36	0.47	0.00	0.28	0.39
FeO*	83.96	74.58	84.01	80.97	48.69	54.11	45.77
MnO	0.46	0.57	0.55	0.46	0.35	0.38	0.35
MgO	2.92	2.23	2.16	2.78	4.55	3.52	3.77
ZnO	0.00	0.00	0.00	0.42	0.00	0.52	0.00
Total	100.00	100.00	100.00	100.00	100.00	100.00	100.00
Cations							
Ti	0.26	0.55	0.30	0.36	1.70	1.56	1.84
Al	0.15	0.13	0.12	0.12	0.06	0.02	0.02
Cr	0.00	0.00	0.00	0.00	0.00	0.00	0.00
V	0.02	0.02	0.01	0.01	0.00	0.02	0.00
Fe3+	1.32	0.76	1.27	1.16	0.56	0.84	0.30
Fe2+	1.07	1.43	1.16	1.18	1.34	1.28	1.54
Mn	0.02	0.02	0.02	0.01	0.02	0.02	0.02
Mg	0.17	0.10	0.13	0.16	0.34	0.26	0.28
Zn	0.00	0.00	0.00	0.00	0.00	0.00	0.00
Cation Total	3.01	3.01	3.01	3.00	4.02	4.00	4.00
Parameters							
Fe2+/(Mg+Fe2+)	0.86	0.93	0.90	0.88	0.80	0.83	0.85
Cr/(Cr+Al)	0.00	0.00	0.01	0.00	0.13	0.00	0.00
(Al+Cr)/(Al+Cr+2* Ti+Fe3+)	0.55	0.35	0.52	0.49	0.29	0.40	0.16
Fe3+/(Al+Cr+Fe3+)	0.08	0.07	0.06	0.06	0.01	0.01	0.01
2*Ti/(2*Ti+Al+Cr)	0.28	0.59	0.32	0.38	0.86	0.79	0.92
2Ti/(2Ti+Fe3+)	0.78	0.89	0.83	0.86	0.98	0.99	0.99

Rock types: ob = olivine basalt; an = andesite; dc = dacite; rh = rhyolite; rb = biotite rhyolite

Minerals: cr = chromite; cr–mt = chromian magnetite; al–mt = aluminian chromite; mt = titanomagnetite; il = ilmenite

* Fe reported as FeO

Table 5: Average Oxide Compositions, Cation Assignments and Parameters (Cont.)

	#47	*SAD24*	*SED05*	*SMPR06*	*SLPR14*	*SLPR13*	*#48*
Mineral	il	il	il	il	il	il	il
Rock	an	dc	dc	rp	rh	rh	rb
Probe	old	old	old	old	old	old	old
No. of analyses	n = 8	n = 4	n = 15	n = 14	n = 5	n = 13	n = 4
Oxides							
TiO_2	44.04	46.71	39.33	38.37	36.58	42.54	51.53
Al_2O_3	0.54	0.59	0.53	0.72	0.50	1.88	0.48
Cr_2O_3	0.00	0.00	0.00	0.00	0.00	0.00	0.00
V_2O_3	0.30	0.00	0.00	0.21	0.32	0.00	0.00
FeO*	51.06	48.60	55.99	56.61	59.88	50.64	36.53
MnO	0.75	0.52	0.63	0.66	0.52	2.39	9.98
MgO	2.96	3.58	3.52	3.43	2.19	2.54	1.10
ZnO	0.34	0.00	0.00	0.00	0.00	0.00	0.38
Total	100.00	100.00	100.00	100.00	100.00	100.00	100.00
Cations							
Ti	1.68	1.76	1.50	1.48	1.42	1.62	1.96
Al	0.04	0.04	0.04	0.04	0.04	0.12	0.04
Cr	0.00	0.00	0.00	0.00	0.00	0.00	0.00
V	0.00	0.00	0.00	0.00	0.00	0.00	0.00
Fe3+	0.60	0.46	0.96	1.00	1.10	0.66	0.08
Fe2+	1.42	1.46	1.22	1.18	1.24	1.32	1.44
Mn	0.04	0.02	0.02	0.02	0.02	0.10	0.44
Mg	0.22	0.28	0.28	0.26	0.18	0.20	0.08
Zn	0.00	0.00	0.00	0.00	0.00	0.00	0.00
Cation Total	4.00	4.02	4.02	3.98	4.00	4.02	4.04
Parameters							
Fe2+/(Mg+Fe2+)	0.86	0.85	0.82	0.82	0.88	0.87	0.95
Cr/(Cr+Al)	0.00	0.00	0.00	0.00	0.00	0.00	0.00
(Al+Cr)/(Al+Cr+2* Ti+Fe3+)	0.30	0.24	0.44	0.46	0.57	0.33	0.05
Fe3+/(Al+Cr+Fe3+)	0.01	0.01	0.01	0.01	0.01	0.03	0.01
2*Ti/(2*Ti+Al+Cr)	0.85	0.88	0.76	0.75	0.72	0.83	0.98
2Ti/(2Ti+Fe3+)	0.99	0.99	0.99	0.99	0.99	0.96	0.99

Rock types: ob = olivine basalt; an = andesite; dc = dacite; rh = rhyolite; rb = biotite rhyolite

Minerals: cr = chromite; cr–mt = chromian magnetite; al–mt = aluminian chromite; mt = titanomagnetite; il = ilmenite

* Fe reported as FeO

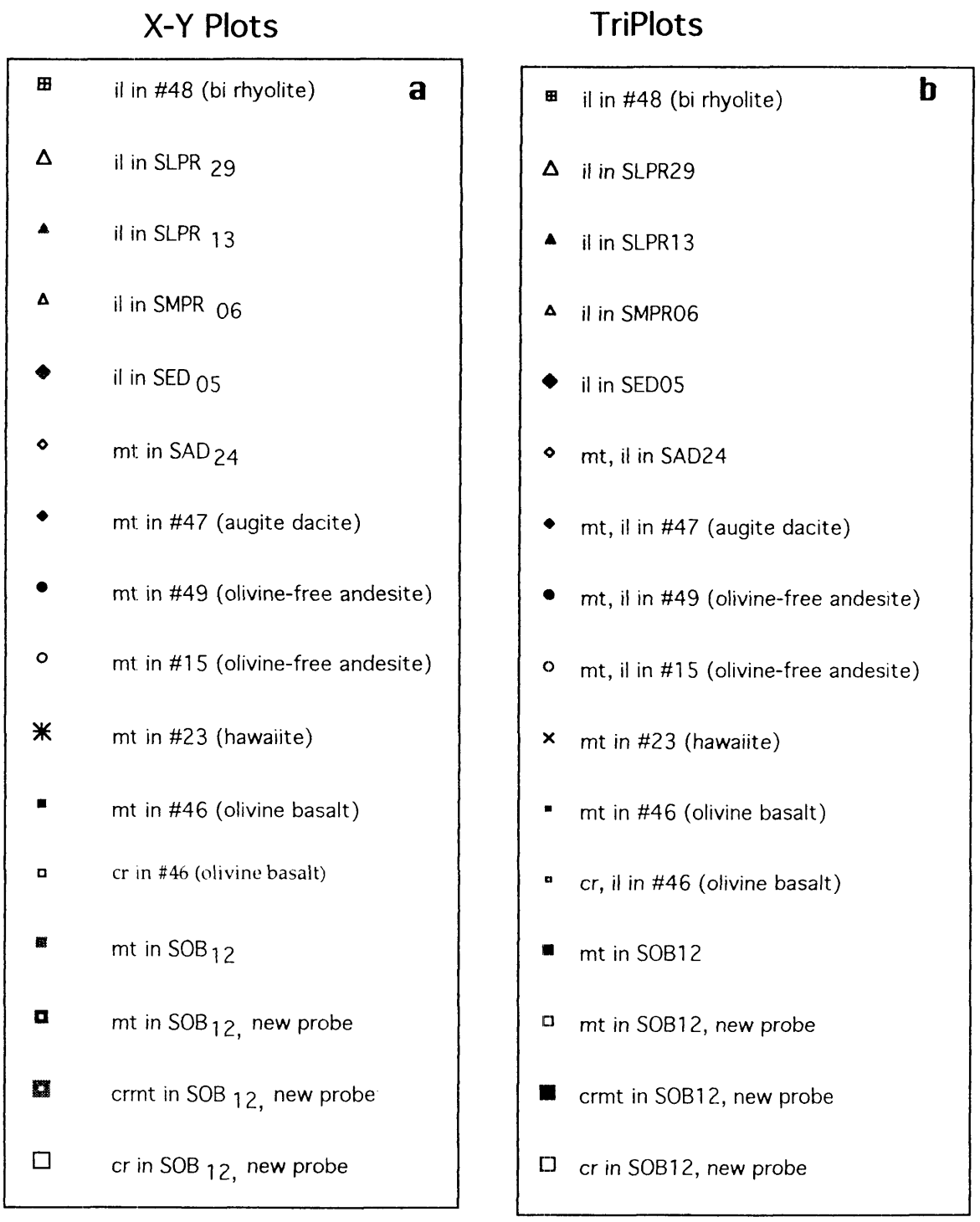

Fig. 22 (a–b): Oxides. Legends used for oxide diagrams (Fig. 22c–t) — X–Y plots (a) and triangular diagrams; (b) minor discrepancies due to limitations of TriPlot software, and due to the need for clarity in X-Y plots. Mineral key: il = ilmenite; mt = magnetite; cr–mt = chromian magnetite; cr = chromite.

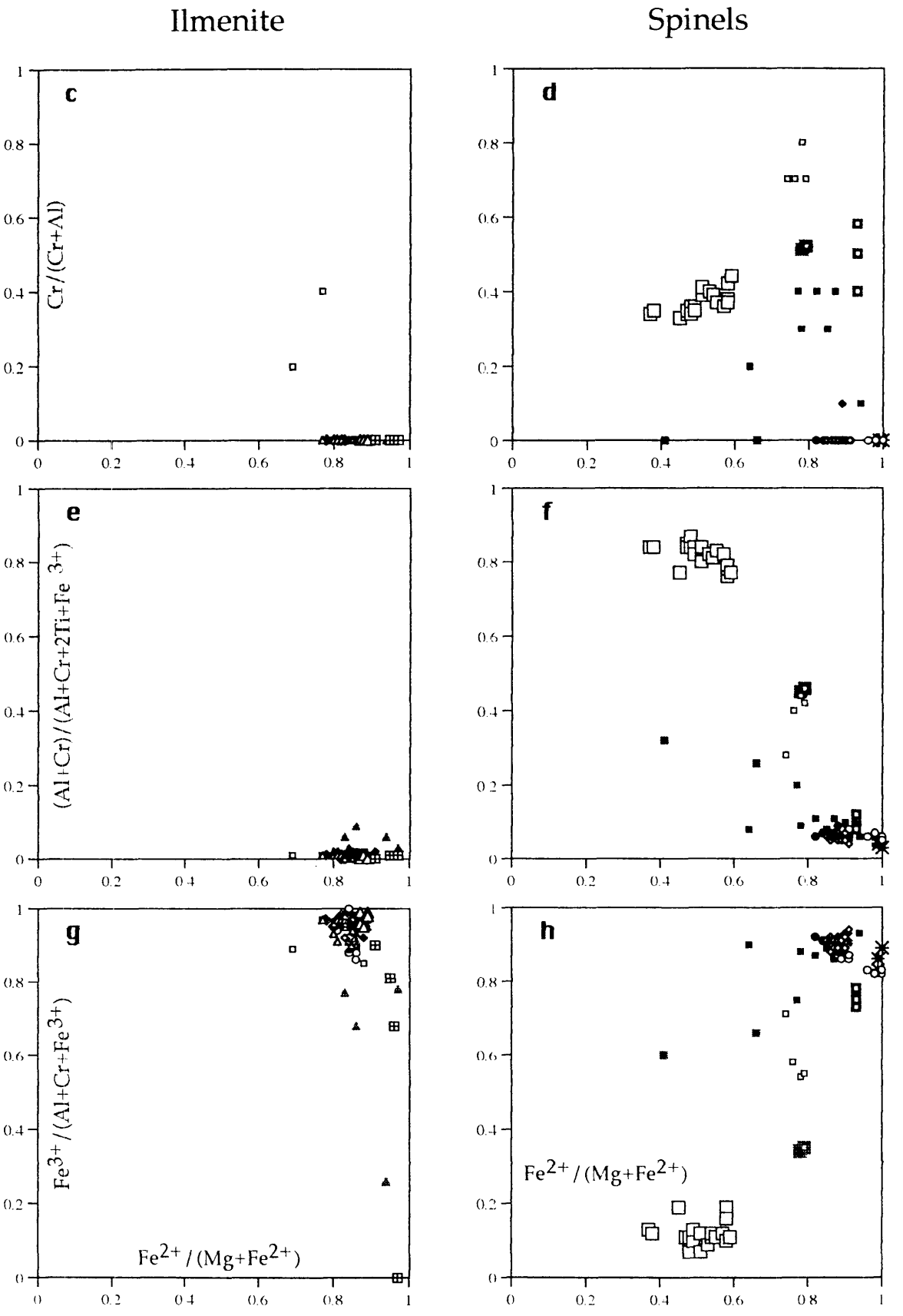

Fig. 22 (c–h): Ilmenite (left) and spinels (right) from the Boggabri Volcanics. See Fig. 22 (a–b) for legend, and text for explanation. Blank abscissae labels as for abscissa label to left; blank ordinate labels as for ordinate label below.

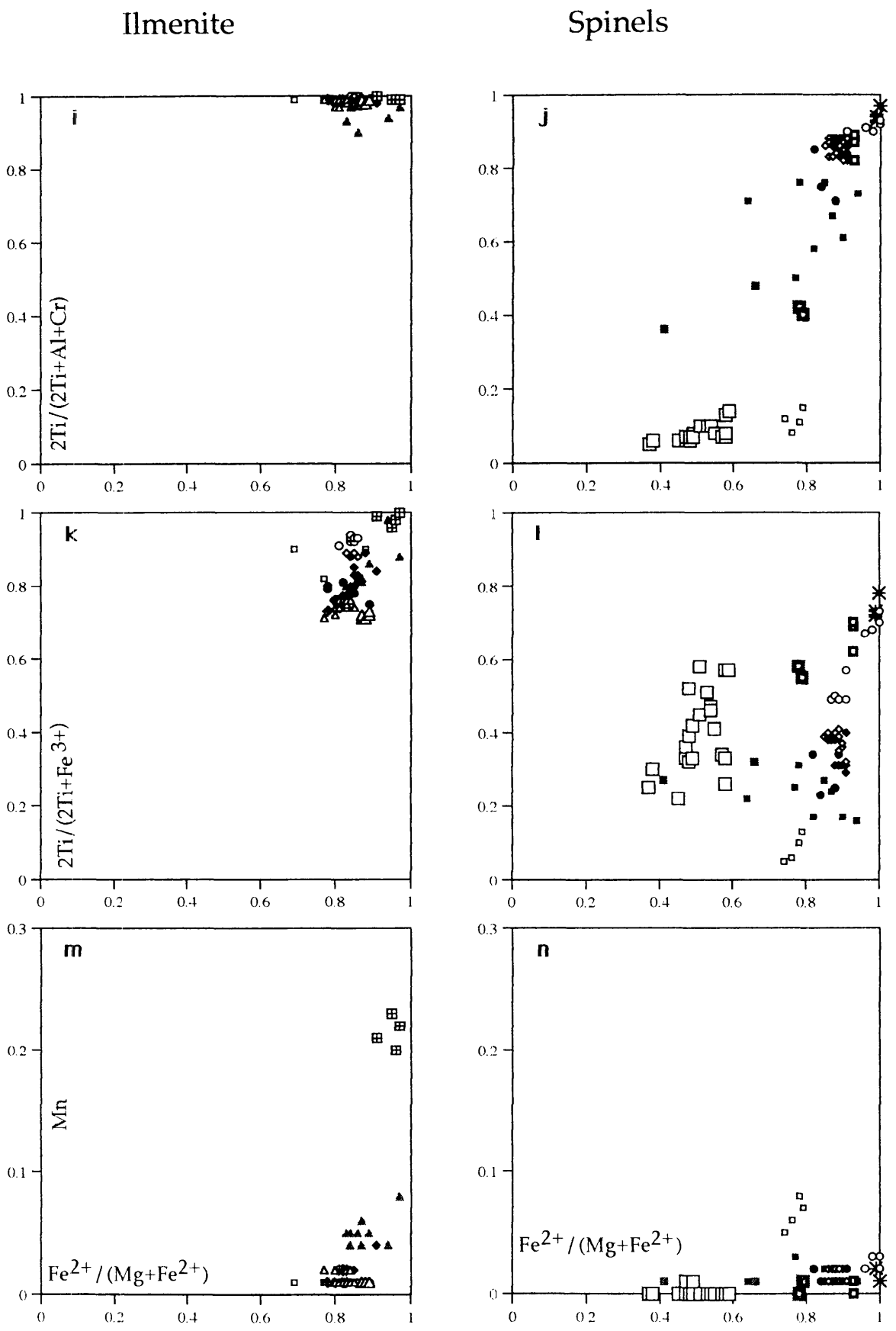

Fig. 22 (i–n): See Fig. 22 (a–b) for symbol legend, Fig. 22 (b–h) for layout details.

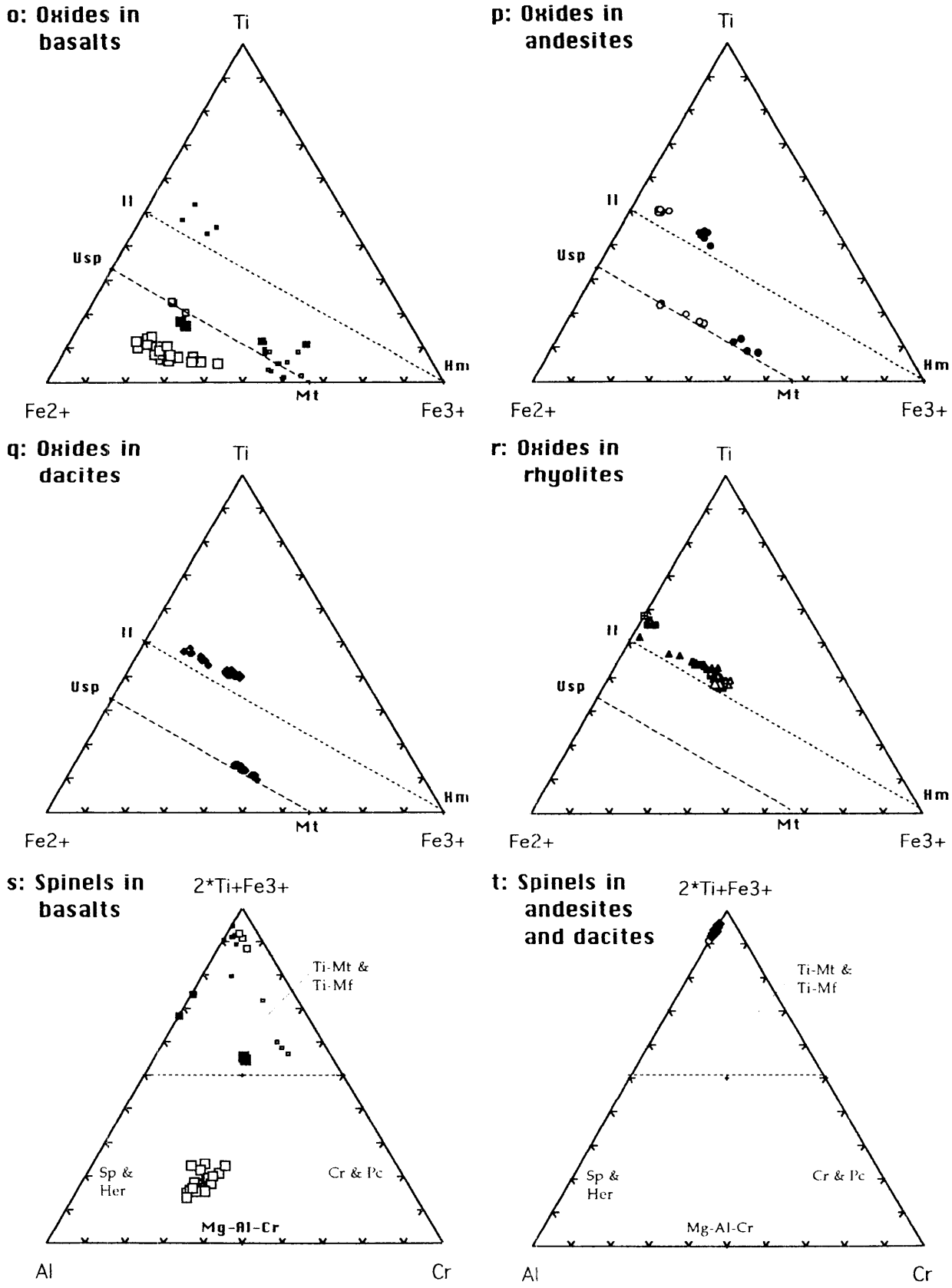

Fig. 22 (o–t): Classification of titanomagnetites and spinels from Boggabri Volcanics. See Fig. 22a–b for graphic legend. Mineral key: Il = ilmenite; Hm = hematite; Usp = ulvospinel; Mt = magnetite; Ti-Mt = titanomagnetite; Ti-Mf = titano-magnesioferrite; Sp = spinel; Her = hercynite; Cr = chromite; Pc = picrochromite.

Fig. 22 c–n shows that most ilmenite and titanomagnetite contains < 25% Mg/Mg+ Fe^{2+}. Only Mg-Al-chromite (new probe) and aluminian titanomagnetite (old probe) from SOB_{12} are consistently more magnesian with Mg/Mg+ Fe^{2+} in the chromite ranging from 0.37 to 0.59.

Chromite contains (a) slightly more Al than Cr; and (b) far more Al+Cr than 2*Ti+Fe^{3+} (average 82% Al+Cr/Al+Cr+2*Ti+Fe^{3+}). These data distinguish the chromite from titanomagnetite, and together with high Fe^{2+} relative to divalent cations establish their identity as Mg-Al chromite (Haggerty, 1976). Chromite contains negligible MnO.

Titanomagnetite contains: (a) significant Cr relative to Al in olivine basalts (up to 80% Cr/Cr+Al) but virtually nil in most other rocks; (b) significant Al+Cr relative to 2*Ti+Fe^{3+} (up to 40% Al+Cr/$\sum$Al+Cr+2*Ti+Fe^{3+}) in olivine basalt, but very little in other rocks; and (c) generally more magnetite component than ulvospinel except in #15 (Usp 49 to 73%), although abundances vary considerably. Fig. 22d shows that the Cr/Cr+Al range in titanomagnetites is extreme, with those in #46 being chromian (up to 80%) and some in SOB_{12} (old probe data) being extremely aluminian (zero Cr, and needing confirmation). Subordinate Al+Cr relative to 2*Ti+Fe^{3+} (Fig. 22f) establishes that the chromian titanomagnetite is not chromite (cf Haggerty, 1976, Fig. Hg–24). MnO in spinels is negligible except for anomalously low values in chromian titanomagnetite from #46.

Ilmenite generally exhibits: (a) very low Cr/Cr+Al (Fig. 22c); (b) very low Al+Cr relative to 2*Ti+Fe^{3+} (Fig. 22e); (c) highly variable Fe3+ relative to Cr+Al (Fig. 22g); (d) very high Ti relative to Cr+Al (Fig. 22i); and (e) high Ti relative to Fe3+ (70 to 100% Il, average 80%). MnO in ilmenite is generally negligible, but is significant in $SLPR_{13}$ and #46 (> 2%) and is concentrated in biotite rhyolite (about 10%).

The following apparent trends in titanomagnetite compositions accompany increasing Fe^{2+}/Mg+Fe^{2+} in oxides from the Boggabri Volcanics: (a) a slight increase in Cr/Cr+Al in olivine basalt followed by a decline to negligible values among intermediate to felsic rocks; (b) a steep decline in Al+Cr/(Al+Cr+2*Ti+Fe^{3+}); (c) steep increases in both Fe^{3+} and 2*Ti relative to Al+Cr. Neither 2*Ti/2*Ti+Fe^{3+} nor MnO exhibit clear trends. In contrast, ilmenite exhibits no change in Cr/Cr+Al or in Cr+Al relative to 2*Ti+Fe^{3+} or 2*Ti/2*Ti+Al+Cr, but exhibit a steep decline, particularly among intermediate to felsic rocks for Fe^{3+}/Al+Cr+Fe^{3+}, a minor increase in 2*Ti/2*Ti+Fe^{3+} and a steep increase in MnO among rhyolites.

Olivine Basalt

Acceptable ilmenite data are only available from #46, although observations using a

back-scattered electron detector on the new probe demonstrate the presence of ilmenite and/or titanomagnetite grains in the groundmass of SOB_{12}. Compositions in #46 are approximately Il_{82-90}, but are slightly displaced above the hematite-ilmenite join (consistent with minor oxidation).

Chromite data are only available from SOB_{12} (new probe) and are as described above. These data plot distinctly below the ulvospinel-magnetite join on Ti-Fe^{2+}-Fe^{3+} (Fig. 22m), reflecting a significant component of low Ti-low Fe spinel. They plot in the imprecisely defined Mg-Al chromite field on 2*Ti+Fe^{3+}-Al-Cr (Fig. 22q).

Titanomagnetite in olivine basalt is diverse and includes chromian titanomagnetite, aluminian titanomagnetite and titanomagnetite that is low in both Cr and Al. Aluminian titanomagnetite projects between Usp_{16-31} on the ulvospinel-magnetite join (Fig. 22g), and plots slightly above the join. Chromian titanomagnetite and titanomagnetite range from about 80% ulvospinel to nearly pure magnetite and plot either side of the Usp-Mt join (Fig. 22m). Aluminian titanomagnetite in SOB_{12} is anomalous in containing negligible Cr.

All ilmenite and most spinel exhibits low MnO. Chromian titanomagnetite in #46 is exceptional and average about 2.1% MnO.

The co-existence of titanomagnetite averaging Usp_{23} and ilmenite averaging Il_{86} in #46 implies equilibration at about log fO_2 of -14 @750°C (cf Haggerty, 1976). The large range in Usp content of titanomagnetite would be consistent with varied equilibration conditions.

Andesites

Two andesites (#49, and #15) together exhibit ranges in ilmenite from Il_{94-75}, and titanomagnetite in the range Usp_{23-73}. MnO contents are uniformly low in ilmenite and titanomagnetite.

The co-existence of the above titanomagnetite and ilmenite ranges implies equilibration under conditions ranging from log fO_2 of -12 @ 950C to log fO_2 more oxidising then -8 @ > 1100°C.

Dacites

Augite dacite (SAD_{24} and #47) contains ilmenite in the range Il_{81-89}, and titanomagnetite in the range Usp_{32-41}, whereas SED_{05} contains only ilmenite which is in the range Il_{73-77}. MnO contents are uniformly low in ilmenite and titanomagnetite.

The composition of coexisting ilmenite and titanomagnetite in SAD_{24} implies

equilibration in the range log fO_2 of -14.5 @ 770°C to log fO_2 of -12 @900°C.

Rhyolites

Ilmenite exhibits an extended range from Il_{71-100}. Values of Il_{100} in #48 are suspect as they are displaced from the ilmenite-hematite join towards the Ti apex (Fig. 22j), and this trend is not readily attributable to oxidation. MnO is slightly concentrated in $SLPR_{13}$ (about 2.4%) and is strongly concentrated in #48 (biotite rhyolite with about 10% MnO).

Summary

The notable features of opaque oxides from the Boggabri Volcanics are the common co-existence of ilmenite and titanomagnetite, the wide range of those compositions, and the correspondingly wide range of inferred temperatures and oxygen fugacities, the limited development of chromian titanomagnetite and Mg-Al-chromite in olivine basalt, and the high MnO content in biotite rhyolite, but generally very low content in other rocks. The inferred oxygen fugacities are generally above the Nickel-Nickel Oxide buffer (Lindsley, 1976), except for the most reduced grains in SAD_{24}, which are slightly below.

GLASSES

Table 6 and Fig. 23a–n summarise the chemistry of groundmass glasses from SED_{05}, $SMPR_{06}$ and $SLPR_{29}$, as well as glass inclusions from plagioclase in the latter. Both old probe data and ANU data are available for $SLPR_{29}$, whereas only old probe data are available for the other two samples. Available data are restricted to major elements, apart from data on BaO and SrO from the ANU probe. MnO and MgO are zero for all but ANU probe data, so these are not plotted in any diagram. The ANU data were obtained using a WDS detector operated at 40 to 45 nA with the beam rastered over an area of 12 µm x 12 µm, whereas the old probe data were obtained using an EDS detector and 1 nA beam current focussed as a 1 µm spot.

No *a priori* acceptance criteria have been applied to glass analyses, because of their uncertain volatile contents, Fe^{3+}/Fe^{2+} ratios, and the lack of applicable stoichiometric criteria for constraining composition. Analyses have been recalculated to volatile-free compositions, but are otherwise unchanged.

Glass data are presented graphically as for whole-rock geochemistry. Pairs of diagrams are used. One of each pair shows all data points, along with average compositions for each set. This one also indicates the Main Trend (including its Intermediate and Felsic Segments) identified in whole rock geochemical analyses (see

Table 6: Analysed and Recalculated Average Glass Compositions

Sample	*Data*	SiO_2 %	TiO_2 %	Al_2O_3 %	*FeO* %	*MgO* %	*CaO* %	Na_2O %	K_2O %
SLPR29	Glass inclusions (ANU probe)	79.72	0.26	13.89	1.08	0.18	0.61	0.20	3.69
	Glass inclusions (old probe)	79.32	0.19	12.90	0.85	0.00	0.58	1.97	4.21
	Ratio of above	1.01	1.37	1.08	1.27	na	1.05	0.10	0.88
SMPR06	Average groundmass glass	78.91	0.32	14.21	0.93	na	1.86	2.60	1.17
	Corrected composition (1)	79.31	0.44	15.30	1.18	na	1.96	0.26	1.03
	Rescaled composition (2)	76.55	0.42	14.77	1.14	na	1.89	0.25	0.99
	Main Trend Intercept (3) (original composition)	74.60	0.42	14.77	1.22	na	0.41	5.40	3.50
	Difference*	1.95	0.00	0.00	-0.07	na	1.48	-5.15	-2.51
	Relative difference*	2.61	0.00	0.00	-6.15	na	358.76	-95.28	-71.70
SED05	Average groundmass glass	78.73	0.32	14.15	0.94	na	2.44	1.42	2.00
	Corrected composition (1)	79.13	0.44	15.24	1.19	na	2.57	0.14	1.75
	Rescaled composition (2)	76.72	0.42	14.77	1.16	na	2.49	0.14	1.70
	Main Trend Intercept (3) (original composition)	74.57	0.42	14.77	1.22	na	0.42	5.40	3.49
	Difference*	2.14	0.00	0.00	-0.07	na	2.07	-5.26	-1.79
	Relative difference*	2.87	0.00	0.00	-5.46	na	491.04	-97.41	-51.36

* Difference = original composition (3) – rescaled composition (2)

Relative difference – 100 * difference/original composition

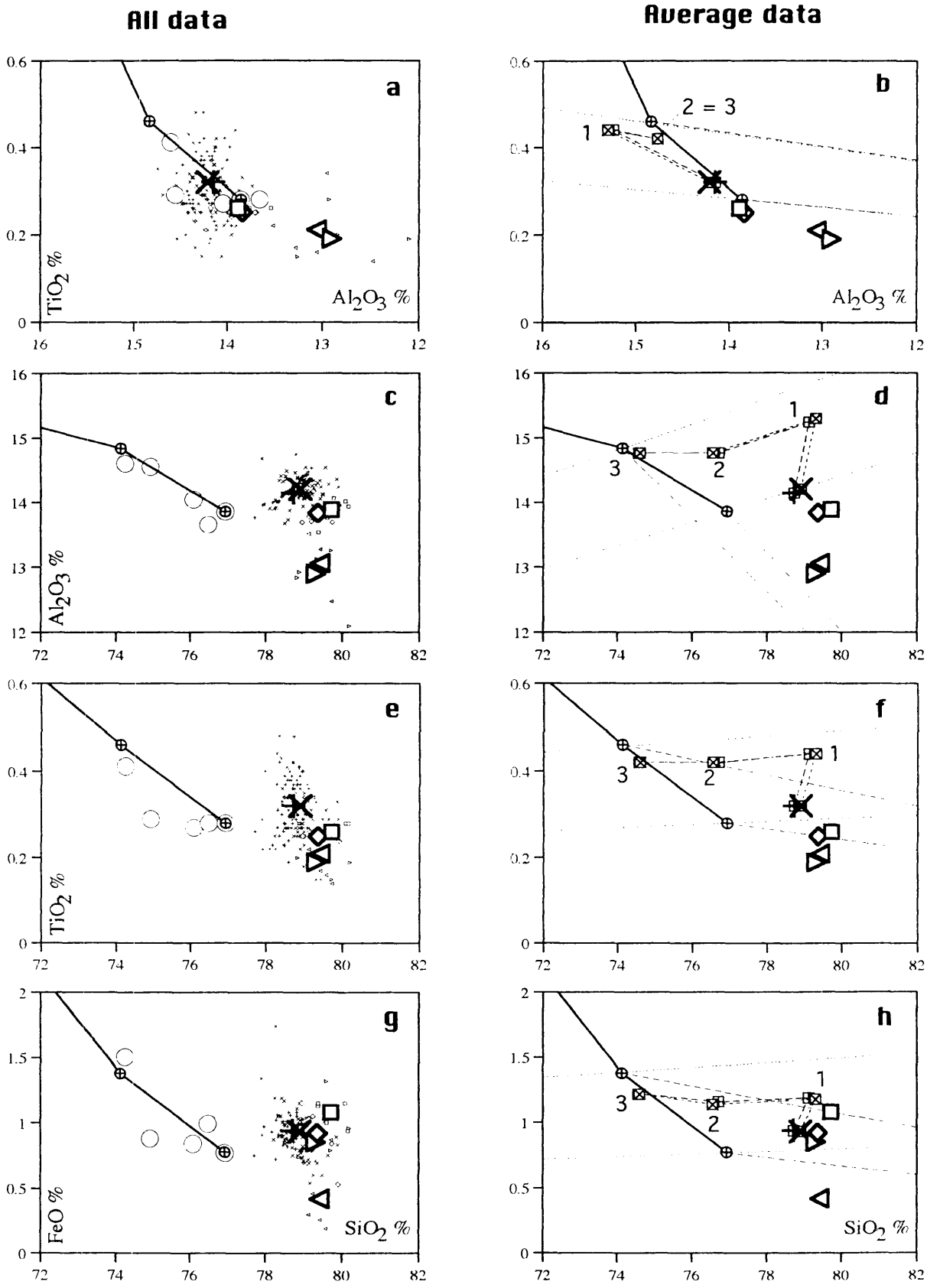

Fig. 23 (a–h): Glass chemistry in relation to Main Trend, silicification trend (joins to 100% quartz) and immobile element trend (joins to zero intercept for both axes). See Figure 23 (o) for symbol legend. Blank abscissae labels as for abscissa label to left; blank ordinate labels as for ordinate label below.

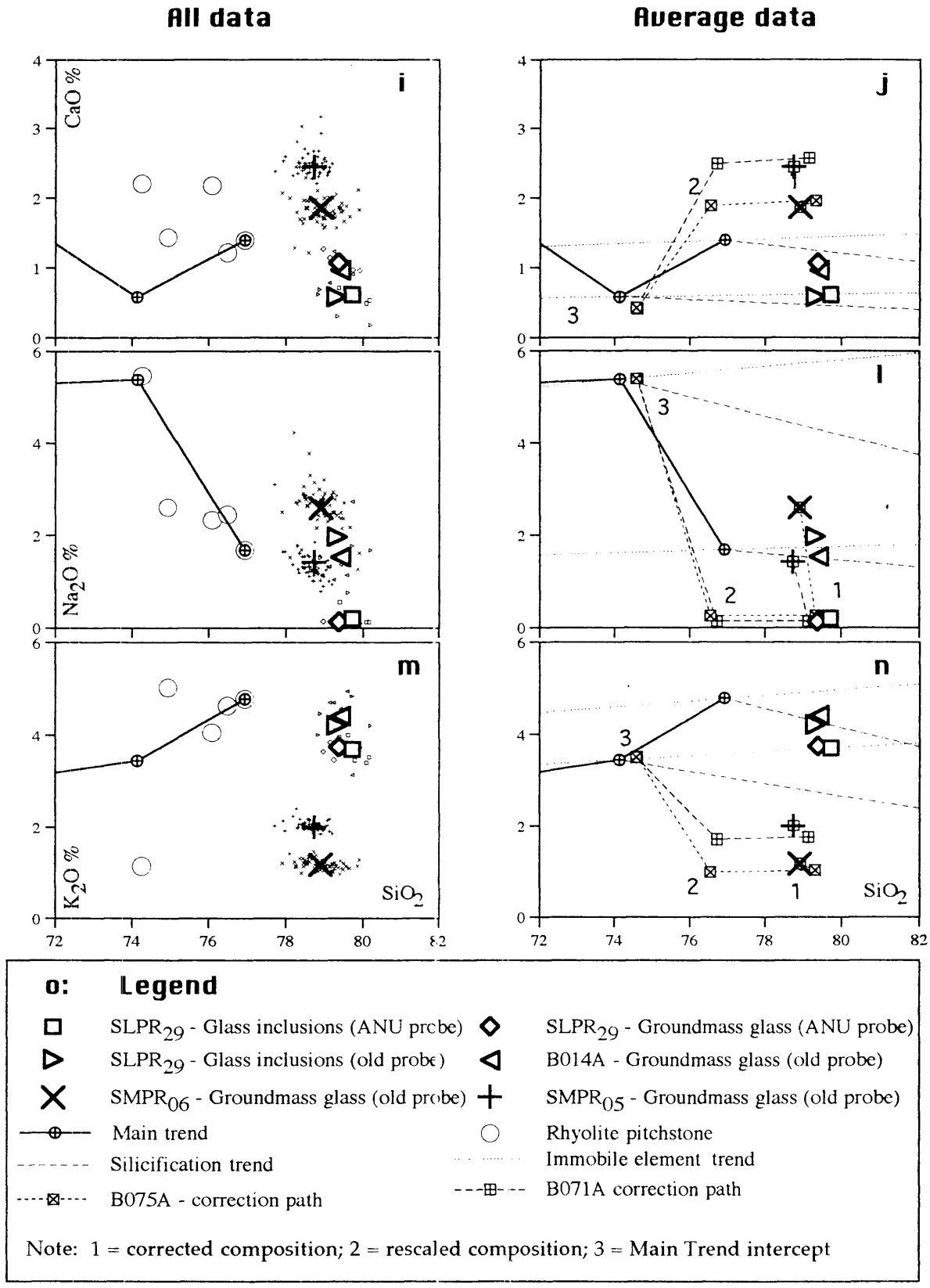

Fig. 23 (i–o): Glass chemistry (cont.)

Geochemistry chapter for definitions), as well as whole-rock rhyolite pitchstones compositions for comparison. The second diagram of each pair shows the average composition for each set, as well as the Main Trend, overprinted by the trend of silicification (mixing line joining to 100% SiO_2) and the trend of apparent concentration/ dilution for immobile elements (mixing line joining to zero — MacLean, 1990). Both silicification and immobile element trends have been drawn from either end of the Felsic Segment of the Main Trend. The second diagram of each pair also presents an attempt to correct for analytical irregularities and possible alteration of the glass in SED_{05} and $SMPR_{06}$.

Overview

The four glass compositions are together characterised by high SiO_2 in a narrow range from 79 to 80% and by more modest values, but significantly greater ranges of values for TiO_2, Al_2O_3, FeO, CaO, Na_2O and K_2O. These silica values are significantly higher that of the Felsic Segment of the Main Trend, and are especially high by comparison with fresh rhyolite glasses (Mahood and Hildreth 1983). Most other oxide ranges are 0.5 to 1.5 times the range of the Felsic Trend, and the ranges partly overlap the ranges of the Felsic Segment. CaO (most analyses) and K_2O ($SMPR_{06}$ and SED_{05}) are significant in being the only oxides that overlap the range of the Intermediate Segment (off diagram in part).

K_2O is notable for an extended range from values comparable to the Felsic Trend in $SLPR_{29}$ to much lower values in SED_{05} and $SMPR_{06}$. The latter, especially that in $SMPR_{06}$ (1.17%) are exceptionally low for felsic igneous rocks (cf BVSP, 1981).

ANU Probe v Old Probe Data for $SLPR_{29}$

Fig. 23 indicates significant systematic differences between ANU probe data and old probe data for both glass inclusions and groundmass glass from $SLPR_{29}$. For example, compared to ANU data for glass inclusions, the old probe indicates compositions that are lower in SiO_2 (0.4%), TiO_2 (0.07%), Al_2O_3 (0.99%), FeO (0.23%), MgO (0.18%), CaO (0.03%) but higher in Na_2O (1.77%) and K_2O (0.52%). Low Na on the ANU probe could be due to volatilisation under the high beam current used with a WDS detector (Neilson and Sigurdson, 1981). This is less likely to occur under the much lower beam current used in the old probe. Some of the smaller discrepancies could be due to sampling bias. However, all old probe MgO results are below detection, and this plus the large differences for Al_2O_3 and K_2O are unlikely to be due to sampling. The new probe at UNE is not yet sufficiently well calibrated to arbitrate.

Geological reasons for this discrepancy are not apparent, as the glass sets analysed

on the two probes would appear to be identical. The differences (other than Na) are most likely due to calibration problems at such high SiO_2 in one of the probes. The difficulties are tentatively attributed to the old probe, in view of the well established reputation of the ANU probe, the extensive testing carried out on it, and the fact that the old probe at UNE was largely calibrated against it.

For this reason, the ratio of ANU to old probe data is used to rescale the average major element compositions for SED_{05} and $SMPR_{06}$ (see Table 6, Fig. 23).

Glass Inclusions v Groundmass Glass in $SLPR_{29}$

Fig. 23 indicates that glass inclusions and groundmass in $SLPR_{29}$ are very similar in composition. Average SiO_2, Al_2O_3, TiO_2 and K_2O contents (about 95% of total composition) are virtually identical. Similarity on $\mathbf{Al_2O_3}$ **v** $\mathbf{TiO_2}$ is particularly significant because these are the most immobile of the major elements. By average old probe data, glass inclusions (brown coloured) contain slightly less SiO_2 (0.1%), TiO_2 (0.02%), Al_2O_3 (0.16%), and K_2O (0.2%) than groundmass glass (greenish and perlitic). However, glass inclusions contain significantly less CaO (0.38%), and significantly more FeO (0.43%) and Na_2O (0.44%). By average ANU probe data, glass inclusions contain more SiO_2 (0.35%), TiO_2 (0.01%), Al_2O_3 (0.05%), FeO (0.16%), MgO (0.08%), and Na_2O (0.07 %), but less CaO (0.46%) and K_2O (0.05%). Thus less CaO in the glass inclusions is common to both probes. Very low Na_2O in both glasses by the ANU probe accounts for the decreased difference between them by that probe. The difference in SiO_2 and Al_2O_3 are trivial compared to the total concentrations of those elements. That leaves only differences in FeO between the two probes unexplained.

Enstatite Dacite (SED_{05}) v Melanocratic Pyroxene Rhyolite ($SMPR_{06}$)

Fig. 23 indicates that SED_{05} and $SMPR_{06}$ are virtually identical in Al_2O_3, TiO_2, SiO_2 and FeO values and in $\mathbf{Al_2O_3}$ **v** $\mathbf{TiO_2}$ relationships. However, $SMPR_{06}$ contains significantly more Na_2O (1.22%), whereas SED_{05} contains significantly more CaO (0.58%), and K_2O (0.83%). TiO_2, Al_2O_3, and FeO are all within the range of the Felsic Segment. CaO values are higher than in the Felsic Segment whereas K_2O is significantly lower. Na_2O differs between the two glasses: $SMPR_{06}$ is higher and SED_{05} is lower than the Felsic Limit of the Main Trend. In general these glasses differ more from the Intermediate Segment of the Main Trend than from the Felsic Segment.

Alteration

To test whether alteration could account for the above anomalous composition, the

following calculations have been carried out on the two averages (see Fig. 23a–n):

a. The value of each component in the two glass compositions has been multiplied by the ratio of the ANU probe value to that of the old probe value for the same component in glass inclusions in $SLPR_{29}$ (point 1 on each diagram). The intent here is to use the ANU data to rescale the old probe data for these two glasses. An alternative technique of adding the difference between the two probe results is not used as Na_2O for SED_{05} would project to a negative value.

b. The values of the two glasses on **Al_2O_3 v TiO_2** have been projected along a line from the origin to intersect the Intermediate Segment (point 2 on Fig. 23a–n). This procedure follows MacLean (1990). It depends on the fact that during bulk alteration, pairs of immobile elements maintain constant ratios and therefore apparently change concentration along radii from the origin on X-Y plots. In both cases the factor is about 0.96 (i.e. indicating apparent concentration of Point 1 relative to Point 2 due to about 4% net mass loss in alteration). TiO_2 could have been used instead of Al_2O_3, but would be more error prone due to far lower abundance.

c. The ratio of point 2 to point 1 has been calculated and used to rescale each other element (point 2 on the other diagrams). The analysis 'totals' about 96.5%, and the deficiency of about 3.5% indicates net mass loss during alteration.

d. Point 2 has then been projected at constant Al_2O_3 to intersect the Intermediate Segment of the Main Trend to yield an estimate of the original composition (point 3; identical with point 2 on **Al_2O_3 v TiO_2**). Theoretically, the sum total of components should now be 100% and departures from 100% provide a measure of cumulative error in the procedure. In this case, the result is slightly low (99.5%). Lack of MgO data and possible volatilisation of Na on the ANU probe could account for this.

e. Mass changes are then calculated from the difference between point 2 and point 3 (Table 6). For $SMPR_{06}$, these are SiO_2 (+1.94%), FeO (-0.21%), CaO (+1.47%), Na_2O (-5.12%) and K_2O (-2.47%) for a net loss of approximately 4%.

f. Relative mass changes are then calculated from the mass change as a percentage of the calculated original composition. For $SMPR_{06}$, these are greatest for CaO (+350%), significant for Na_2O (-95%) and K_2O (-72%), but is small for other oxides (e.g., +2.6% for SiO_2).

g. A similar procedure applied to SED_{05} yields a similar mass change and almost identical original composition (consistent with their similar Al/Ti values).

A similar procedure, but without first correcting for discrepancies between ANU and old probe data, would yield anomalously high SiO_2 and low Al_2O_3, and significantly

lower TiO_2 and FeO. CaO, K_2O, and Na_2O would be virtually unaffected despite the complex correction geometry.

Original Glass

The glass composition calculated for both SED_{05} and $SMPR_{06}$ is that of a low-Si rhyolite with 74% SiO_2 and lying on the extension of the Intermediate Segment not far from the Felsic Inflection.

Summary

Original glasses in SED_{05} and $SMPR_{06}$ are probably identical and of low-Si rhyolite composition slightly more siliceous that the Felsic Inflection, but less siliceous (2.6 to 2.9%) than the analyses glasses. As the analysed glasses are the dominant component in the host rocks, bulk compositions have probably changed by similar amounts. It should however, be noted that SED_{05} was a component in the definition of the Intermediate Segment, and the validity of that trend needs independent corroboration.

OVERALL SUMMARY

Significant alteration in two sets of glass analyses suggests that all pitchstones have probably undergone similar alteration affecting both their glass and bulk chemistries.

Mineral chemistry indicates that olivine in basalts have typical MORB compositions, and overlap the OIT range and the more primitive range of CFBs (BVSP, 1981; Wilson, 1989). Plagioclase resembles MORB both in its An range and especially in its low Or content, which distinguishes it from OIT, continental and arc suites (BVSP, 1981). Chromite and titanomagnetite are arc-like or like some Hawaiian types due to low Mg which also distinguishes them from MORB analyses. Augite is N-MORB or arc-like, but lacks the Fe-enrichment of evolved tholeiites (E-MORB, OIT, CFB), and is not as primitive as Hawaiian or MORB megacrysts (BVSP, 1981). Enstatite and olivine also lack significant Fe-enrichment that is common in evolved tholeiites. In contrast, MnO is enriched in ilmenite and enstatite in some leucocratic rhyolites. Biotite data all failed quality control, but X-Ray spectra indicate the probable presence of significant fluorine.

Oxygen fugacities range broadly from slightly below the Ni-NiO buffer to significantly above it, and is apparently independent of bulk composition; this might be due to environmental factors rather than being an intrinsic property of the rocks.